國立臺灣大學工學院環境工程學研究所

碩士論文

Graduate Institute of Environmental Engineering

College of Engineering

National Taiwan University

Master Thesis

以硫脲改質球狀活性碳進行印刷電路板廢水中金之選擇性吸附

Selective Adsorption of Gold from PCB Wastewater by Thiourea-Modified Activated Carbon Sphere

鄧逸萱

Yi-Hsuan Teng

指導教授：席行正 博士

Advisor: Hsing-Cheng Hsi, Ph.D.

中華民國 109 年 7 月

July 2020

doi:10.6342/NTU202002980

誌謝

時光飛逝，轉眼到了畢業的季節，我也即將從台大環工所畢業。回想其中的酸甜苦辣，即使有許多課業或實驗上的挫折，如今想想，都是灌溉我的各種養分，支持著我前往更好的目的地，內心除了感激還是感激。

感謝席行正教授對我的指導與包容，給尚未明瞭要做什麼題目的我指引了一條明燈，老師對於我的研究總是給予高度的支持與肯定，即使研究上的成果不太好，他也會給我滿滿的鼓勵，讓我能持續向前、不畏艱難的跨越困難，最終完成了我的論文。另外，特別感謝口試委員余炳盛老師、林進榮老師與江右君老師撥冗指導，給予我許多研究上的建議，讓整體研究可以更完整。感謝政諺、煜偈、哲榮、映琳學長姊在實驗上的協助與分析儀器上的幫忙。感謝實驗室的同學：世盈，書聞、安均、奕丞、廷鈞、夢圓，與你們一起討論實驗上的問題，幫我找到許多我沒想到的盲點，夜晚的實驗室有你們的陪伴都不會孤單，大家一起做實驗、寫論文，一起準備口試，雖然累卻過得很充實。感謝與我到台大打拼的大學同學：鈺玲、虹希、靖蕙。在剛到台北還很不適應的時候，照顧我、陪我去看醫生，在課業上互相照應。每天晚上到你們房間聊天是我一天最好的紓壓，互相抱怨彼此的實驗困難，儘管有時各自做自己的事，但有你們在就讓人覺得安心。感謝泓宇，這兩年除了在台北，最常去的地方就是新竹了，新竹也許不比台北繁華，但有你在的地方，總是會留下許多美好的回憶，還好有你常常帶我去打球爬山運動，讓我有更多體力可以做研究。

最後感謝我的父母，讓我沒有金錢上的煩惱，每次回家總是帶我吃大餐，也會常常有空就來台北看我，有你們在背後的支持，是我完成論文的最大動力！

doi:10.6342/NTU202002980

中文摘要

城市採礦，代表著從廢棄電子電機設備(WEEE)產品等回收有價物質，是一種循環經濟的概念。根據文獻顯示，2016 年的廢棄電子電機設備已達到 44.7 百萬噸且預估在 2021 年將成長至 52.2 百萬噸。將資源循環永續利用，在全球越來越受到重視，而對缺乏天然礦產的台灣來說，更是重要的議題。在廢棄電子電機設備中，以印刷電路板(PCB)為例，含有金、銀、鉑等貴重金屬，雖然這些貴重金屬的佔比相對少，但其價值卻相當高；而金在貴金屬中，依據其佔比換算價值，可獲得最高的回收價值。

本研究使用硫脲改質活性球狀碳以吸附方法回收金，首先將碳化過的酚醛樹酯放在直立高溫爐中並通入二氧化碳，經過 4 小時、900°C 的活化後，形成球狀活性碳(ACS)，再將硫脲溶入水與酒精混合溶液，倒入裝好球狀碳的燒杯中，經過 8 小時、60°C 的加熱攪拌後，過濾烘乾而得到硫脲改質活性球狀碳(TUACS)。經過初步選擇性吸附實驗測試中可發現，在含有金、銅、鉛、鋅、鎳的水溶液中，硫脲改質活性球狀碳對金具有選擇性吸附的特性，因此，進一步對於此材料進行物性化性分析，根據元素分析(EA)結果可得知，硫含量從 0 上升至 10%；而 BET 比表面積從 2445.3 m^2/g 下降至 1948 m^2/g，顯示硫官能基成功吸附在球狀活性碳上造成表面積與孔體積下降。經過 XPS 分析，可得知硫官能基可能為 C-S 鍵與亞硫酸鹽離子 sulfite ion (SO_3^{2-})，可協助金離子還原為元素金的鍵結官能基。另外，探討時間、劑量、pH 值對硫脲改質活性球狀碳吸附金的影響，發現達到飽和吸附平衡時間為 96 小時、且在 pH=2、劑量為 0.01 g L^{-1}，其吸附金的回收效率可達 70%左右，而劑量增加至 0.06 g L^{-1} 時，其回收效率可上升至 99%左右。在等溫吸附實驗中，可得知其較符合 Langmuir 等溫吸附曲線。在脫附實驗中，利用 0.3 M 的硫代硫酸銨(ammonium thiosulfate)進行脫附實驗，脫附時間為 24 小時，得到的脫附效率可達到 94%，證實使用硫代硫酸銨脫附元素金為可行方法。最後進行重複吸附與脫附試驗，了解此

doi:10.6342/NTU202002980

材料之重複利用率，經過五次的重複吸脫附，其金回收效率仍可達到 90%，表示此材料很適合重複使用。

關鍵字：活性球狀碳、硫脲、選擇性吸附、金、電子廢棄物

doi:10.6342/NTU202002980

Abstract

Urban mining represents the recycling of valuable materials from waste electrical and electronic equipment (WEEE) products, and it is a concept of circular economy. According to the literature, the waste electrical and electronic equipment in 2016 has reached 44.7 million tons and is expected to grow to 52.2 million tons in 2021. The sustainable use of resources is increasingly important all over the world. For Taiwan, which lacks of natural minerals, sustainable use of resources in waste is even more vital. Among the WEEE, printed circuit boards (PCBs) contain precious metals such as gold, silver, and platinum. Although these precious metals account for a relatively small proportion, their values are very high. Gold is obviously one of the metals with the highest recycling value and worth to be recycled.

In this study, thiourea modified activated carbon sphere (TUACS) was used to recover gold by adsorption. First, carbonized phenol-formaldehyde (PF) resin was carbonized using carbon dioxide in an upright high-temperature furnace at 500^{o}C for 1 h. After 4 hours of activation at 900^{o}C, activated carbon sphere (ACS) is formed. ACS was then immensed in to a mixed solution of DI water and ethanol (EtOH) with thiourea dissolved in. The solution was heated and stirred at 60^{o}C for 8 h, then filtered and dried to obtain TUACS. The selective adsorption experiment tests showed that TUACS has

doi:10.6342/NTU202002980

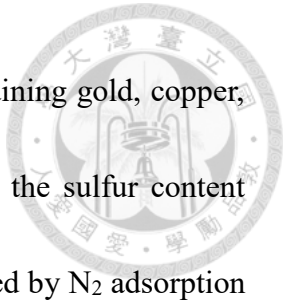

excellent ability to selectively adsorb gold in aqueous solution containing gold, copper, lead, zinc, and nickel ions. Elemental analysis results showed that the sulfur content increased from 0 to 10% and the BET specific surface area determined by N_2 adsorption decreased from 2445.3 to 1948 $m^2\ g^{-1}$, indicating that sulfur functional groups were successfully impregnated in TUACS, causing a decrease in surface area and pore volume. XPS analysis showed that the sulfur functional groups were mainly as C-S bonds or sulfite ion (SO_3^{2-}), which may be the key functional groups that bond and reduce gold ions to elemental gold. The time to reach an adsorption equilibrium of gold was 96 h at pH= 2 with the dosage of 0.01 g L^{-1}, and the gold recovery can reach about 70%. When the dosage increased to 0.06 g L^{-1}, the gold recovery efficiency of TUACS can rise to about 99%. The isotherm adsorption experiments suggest that the gold adsorption by TUACS is better fitted with the Langmuir isotherm than the Freundlich isotherm.by using 0.3 M ammonium thiosulfate ($(NH_4)_2S_2O_3$) to desorb gold, the desorption efficiency could reach 94% in 24 h. These results confirm that the element gold present in TUACS can be successfully desorbed with ammonium thiosulfate. Finally, repeated adsorption and desorption tests indicate that after five repeated adsorption and desorption, the gold recovery efficiency of TUACS can still reach 90%, confirming that the TUACS fabricated

doi:10.6342/NTU202002980

in this study is a novel gold-selective adsorber with high adsorption efficiency and reuse ability.

Keywords：Activated carbon sphere, thiourea, selective adsorption, gold, electronic waste

doi:10.6342/NTU202002980

Contents

doi:10.6342/NTU202002980

doi:10.6342/NTU202002980

doi:10.6342/NTU202002980

doi:10.6342/NTU202002980

doi:10.6342/NTU202002980

List of Figures

doi:10.6342/NTU202002980

doi:10.6342/NTU202002980

doi:10.6342/NTU202002980

List of Tables

doi:10.6342/NTU202002980

Chapter 1 Introduction

1.1 Motivation

Waste electrical and electronic equipment (WEEE) is a growing issue around the world. With technological advancements, industries turn into greater automation, which has increased the electrical and electronic equipment (EEE) usage (Kumar, Holuszko, & Espinosa, 2017). 44.7 million metric tons of WEEE were engendered in 2016, and the quantity of WEEE is expected to grow into 52.2 million metric tons by 2021. However, around 80% of WEEE is not established to be gathered and properly recycled in 2016. The total value of all raw materials present in WEEE is estimated at approximately 55 Billion Euros in 2016 (Baldé et al., 2017). Taking printed circuit board (PCB) as an example, it contains more than ten times higher purity of precious metals, including Au, Pt, Pd, etc., in comparison to the rich ore content. Among these precious metals in PCB, gold is one of the most valuable materials. Therefore, to recovery the precious metals such as gold from WEEE are essentially important with respect to circular economy.

Up to now, there have been several methods for recovery of the gold from wastewater extracted from WEEE. To take a case in point, chemical precipitation, ion exchange, and adsorption are some methods used to recover gold from wastewater (Li, Eksteen, & Oraby, 2018). The chemical precipitation adjusts pH value through introducing alkali, and the

doi:10.6342/NTU202002980

metal ions precipitate in the specific pH value (Yang et al., 2017). Further, the metal could be recovered. The challenge of chemical precipitation is that it consumed a large amount of alkali, which increases the recovery cost. The ion exchange by resin is good at gold recovery, also it has the selectivity characteristic, but the mechanical strength, breakage rate, and abrasion resistance are lower than those of activated carbon (Wu et al., 2017). Moreover, resin may not be suitably used in some severe conditions of wastewater. Adsorption by activated carbon is also a conventional adsorbent for gold recovery, which has fast adsorption rate and large adsorption capacity (Bryson, 1995). Although the selectivity characteristic is not especially excellent, we can modify the activated carbon by some environment-friendly materials to enhance the selective ability of gold recovery.

1.2 Research objectives

The wastewater of PCB production contains precious metals such as gold (Au), base metals (Cu, Zn, etc.), and potential toxic metals (Pb, etc.). It is crucial in selective adsorption to recover gold. In this research, the activated carbon sphere (ACS) was produced and then modified by thiourea (TU) to form the thiourea-modified activated carbon sphere (TUACS). TUACS was used as the adsorbent to selectively separate Au from wastewater containing Cu, Pb, Zn, and Ni ions.

In this study, the optimal TUACS adsorption condition was obtained based on batch experiments. The main objectives of this study are listed as follows;

doi:10.6342/NTU202002980

(1) The activated carbon sphere (ACS) was produced and modified by thiourea (TU) to form the thiourea-modified activated carbon sphere (TUACS). The physical and chemical characteristics of both ACS and TUACS were analyzed.

(2) The influencing valuables including saturated adsorption time, pH value, and TUACS dosage were examined by batch Au adsorption experiments. The adsorption efficiencies of Au by TUACS from wastewater were then investigated and discussed.

(3) The Au desorption efficiency of TUACS by using ammonium thiosulfate at various concentrations was investigated. Then, the repeated adsorption and desorption experiments of Au were conducted to realize the reusability of TUACS.

doi:10.6342/NTU202002980

Chapter 2 Literature Review

2.1 Waste electric and electronic equipment (WEEE)

The term “E-waste” means all types of electrical and electronic equipment (EEE) that have been thrown away by the possessors as waste without intention of reuse (Kumar et al., 2017). E-waste is also named as waste electrical and electronic equipment (WEEE). It comprises a broad range of products that contain six waste categories: (1) temperature exchange equipment, (2) screens and monitor, (3) large equipment, (4) small equipment, (5) small IT and telecommunication equipment and (6) lamps.

44.7 million metric tons of WEEE were engendered in 2016, and the quantity of WEEE is expected to grow into 52.2 million metric tons by 2021. Figure 2-1 shows the collection methods of WEEE in 2016. In brief, around 20% of WEEE is established to be gathered and properly recycled, while 80% of WEEE is not documented in 2016 (Baldé et al., 2017).

doi:10.6342/NTU202002980

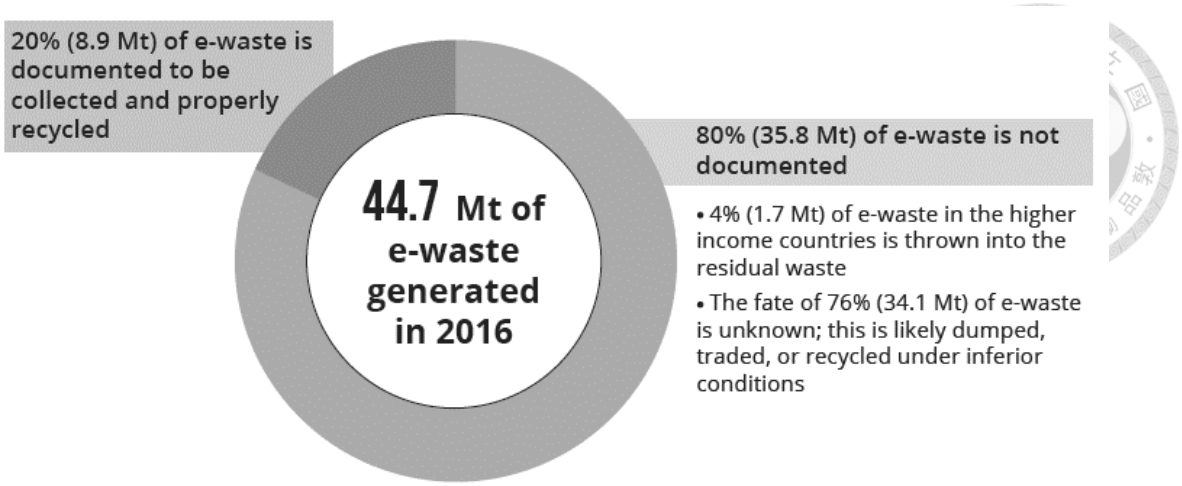

Figure 2-1 Collection methods of WEEE in 2016 (Baldé et al., 2017)

WEEE contains rare earth metals (REM), for example, scandium (Sc), yttrium (Y), and lanthanides (Ce, Pr, Nd). The REMs have applied for their electronics, strength, alloying, and performance properties in electrical and electronic equipment (Tansel, 2017). WEEE also contains precious metals, including gold, silver, platinum, copper, and palladium. Besides, it also consists of valuable bulky materials like iron and aluminum. Also, plastics can be recycled. As shown in Table 2-1, we can determine the potential value of raw materials in WEEE in 2016. In sum, the economic opportunities of secondary materials are valued at least 55 billion Euros in 2016 (Baldé et al., 2017).

doi:10.6342/NTU202002980

Table 2-1 potential value of raw materials in WEEE in 2016

Material	Kilotons (kt)	Million (€)
Au	**0.5**	**18840**
Ag	**1.6**	**884**
Cu	**2164**	**9524**
Fe	**16283**	**3582**
Al	**2472**	**3585**
Pd	**0.2**	**3369**
Plastics	**12230**	**15043**

doi:10.6342/NTU202002980

2.2 Introduction of printed circuit board (PCB)

A printed circuit board (PCB) is an essential platform which supplies mechanically strengthens and electronically interconnects for almost all electronic components (Gajdovcik et al., 2019; Tsai & Chiu, 2007). The manufacture processes of printed circuit boards (PCBs) commonly achieve utilizing a chemical etching process. The most ordinary form of etch used with PCBs is ferric chloride (Zhan & Xu, 2014). Figure 2-2 is a rough attempt to show the fabrication process of PCB (Gröger et al., 2010).

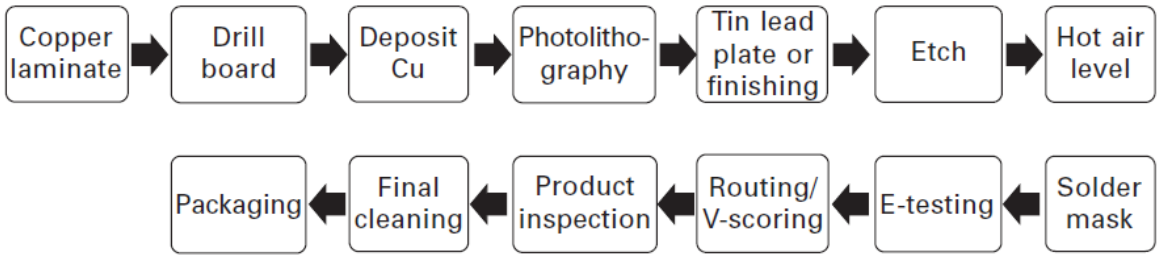

Figure 2-2 Fabrication process of PCB (J. Li & Zeng, 2012)

2.2.1 Metals of waste printed circuit boards (WPCBs)

At a rough evaluation, WPCBs contain one-third of the weight of metals, mainly Cu (10%-27%), Ni (0.3%-3%), Pb (1%-4.5%) and Zn (0.2%-2%) (Zhang et al., 2012). Besides, precious metals like Au (0.039%), Ag (0.156%), and Pd (0.009%), which use as connecting materials or plating layers because of their chemical stability and electric conductivity (Lu & Xu, 2016).

doi:10.6342/NTU202002980

WPCBs contain more than ten times higher purity of precious metals, including Au, Pt, Pd, etc., in comparison to the rich ore content, incurring the attention to extract noble metal from WEEE. Accordingly, the extraction of noble metals from WEEE should be given significant priorities (Islam et al., 2020).

Except for precious metals, high concentrations of heavy metals (Ni, Cd, Pb, and Hg) were confirmed present in the environmental water, which could be attriibuted to the direct effects of WEEE (Yang et al, 2013).

2.2.2 Characteristic of gold

Gold is (1) a good conductor of electricity and heat, (2) hardly affected by exposure to air or most reagents and (3) inert and a good reflector of infrared radiation (Laguna, 2008). Gold also has the lowest electrochemical potential of any metal. In other words, gold in any cationic form will accept electrons from nearly any reducing agent to form metallic gold. More specifically, it is the most electronegative of all metals. The oxidation state of gold between −1 to +5, but Au (I) and Au (III) are in the majority.

doi:10.6342/NTU202002980

2.3 Methods of precious metals recovery from WPCBs

Precious metals were typically separated from WEEE using hydrometallurgical, pyrometallurgical, and electrometallurgical processes. The introduction of these three processes is stated as following sections.

2.3.1 Pyrometallurgy

Pyrometallurgy is a traditional technology for the recovery of non-ferrous metals as well as precious metals from WPCBs. Pyrometallurgy includes incineration, smelting in a plasma arc furnace or blast furnace, drossing, sintering, melting, and reactions in a gas phase at high temperature (Li & Zeng, 2012). The pyrometallurgy process releases hazardous gases, like dioxins, that cause a negative influence in the environment. Aside from this, the pyrometallurgy method dissolves the gold by using a cyanide solution or aqua regia. These two solvents are costly, toxic, and completely non-recyclable. It has to be stressed that the charge to extract 1 kg of gold using aqua regia is $1520 and results in 5000 L of waste (Islam et al., 2020). Although the pyrometallurgy technologies have been improved and upgraded in developing countries, pollution problems are still inevitable. Except for the dioxins issue mentioned above, the release of the $PM_{2.5}$ also needs to pay attention (Ding et al., 2019).

doi:10.6342/NTU202002980

2.3.2 Hydrometallurgy

Hydrometallurgy is a conventional technology for the recovery of precious metals from WPCBs. The main steps in hydrometallurgy are comprised of a series of acid or caustic leaches (cyanide, thiosulfate, thiourea, and halide, etc.) of solid materials. Alkaline conditions were used to leach out the cyanide and thiosulfate, while acidic conditions were used for thiourea and halide leaching (Islam et al., 2020). Table 2-2 provides the list of gold extraction from WPCB by various leaching agents. The solutions are then subjected to separation and purification procedures such as precipitation of impurities, solvent extraction, adsorption, and ion-exchange to isolate and concentrate the metals of interest. Accordingly, the solutions are treated by electrorefining process, chemical reduction, or crystallization for metal recovery (Li & Zeng, 2012). Although the hydrometallurgical process has some drawbacks, leaching process, liquid-liquid extraction, Liquid-oxidant systems have been attracted considerable attention lately.

doi:10.6342/NTU202002980

Table 2-2 Gold extraction from WPCB by various leaching agents.

Material	Leaching conditions	Temp. (°C)	time	Recovery rate	References
PCBs	Iodine 3%, H_2O_2 1%, pH =7	35	4 h	Au 99.98%	(Sahin et al., 2015)
PCBs	Hydrochloric acid solution, thiourea or acidic thiourea	50	2 h	Au 98%	(Choudhary et al., 2018)
PCBs	Thiosulfate 72.71 mmol, Cu^{2+} 10.0mmol, NH3 0.266 mol	40	5 min	Au 91%	(Ha et al., 2014)
PCBs	Aqua regia and iodine/iodide	75	3 h	100% of gold	(Birich et al., 2018)
PCBs	HCl, NaCl, H_2O_2	25	4 h	95.73% gold	(Li et al., 2019)
PCBs	5 vol% HCl, Amberlite XA D-7HP, Bonlite BA304, and Purolite A-500	25	163 min	97% gold	(Kim et al., 2011)

doi:10.6342/NTU202002980

2.3.2.1 Leaching agent: cyanide

Traditional hydrometallurgy processes are composed of cyanide and aqua regia leaching. Precious metal like Au and Ag can be leached in a cyanide solution. The cyanide concentration, oxidant dosage, pH, and temperature significantly affect leaching efficiency (Xie et al., 2014). CN^- dissolves precious metals by complexation because it is an active ingredient. As CN^- is stable at pH=10.2, the optimal pH of the cyanide solution is 10-10.5. Below pH=8.2, highly volatile hydrogen cyanide (HCN) form, leading to severe injuriousness to operators' health (Ding et al., 2019). The chemistry reaction for leaching gold from WEEE by cyanide is shown in Eqs. (2-1):

$$4Au + 8CN^- + O_2 + 2H_2O \rightarrow 4Au(CN)_2^- + 4OH^- \quad (2\text{-}1)$$

2.3.2.2 Leaching agent: thiourea

Modified and new hydrometallurgical technologies have been investigated by several types of research to reduce environmental pollution. Some non-cyanide leaching agents such as thiosulfate, thiourea, and thiocyanate were recommended (Ding et al., 2019).

Thiourea ($CS(NH_2)_2$) is a prospective extracting agent owing to its high leaching rate and eco-efficiency (Ding et al., 2019). The dissolution of gold in a thiourea solution is an electrochemical process. An acidic medium must be used to assure the stability of the thiourea and to avoid it from degrading too speedy (Lacoste-Bouchet, Deschênes, & Ghali, 1998). The Au-thiourea complex form as Eqs. (2-2):

doi:10.6342/NTU202002980

$$Au + 2SC(NH_2)_2 \rightarrow Au(SC(NH_2)_2)_2^+ + 1e^- \qquad E_{std} = -0.38\ V \qquad (2\text{-}2)$$

The electron pairs between nitrogen and sulfur atoms have a better potential for a coordination bond between gold and silver during thiourea leaching. Leaching gold by thiourea may be of crucial importance due to a rapid reaction with gold and low-price, along with less environmental impact competing with cyanide (Lacoste-Bouchet et al., 1998).

2.3.2.3 Leaching agent: thiosulfate

Thiosulphate was derived as another option to cyanide for the extraction of gold from ores. Leaching tests implemented using ammonium thiosulphate solution as a leaching agent engendered relatively low recovery of gold compared to cyanide leaching with relatively higher reactive species consumption (Akcil et al., 2015).

Akcil et al. (2015) stated that gold leaching in a thiosulphate solution accommodating copper and ammonia is an electrochemical reaction as shown in the following Eqs. (2-3).

$$Au + 2S_2O_3^{2-} \rightarrow Au(S_2O_3)_2^{3-} + e^- \qquad (2\text{-}3)$$

Table 2-3 summarizes the pros and cons of potential leaching reagents for gold. Furthermore, the linear correlations of stability constants of Au(I)-complexes follow the order: $CN^- > S_2O_3^{2-} > CS(NH_2)_2$ (Cui & Anderson, 2016).

Table 2-3 Pros and cons of potential leaching reagents for gold (Cui & Anderson, 2016)

doi:10.6342/NTU202002980

2.3.3 Purification of leaching solution

Many alternative technologies for recovering the gold from leaching solutions such as ion exchange by resin, activated carbon adsorption, and electrometallurgical processes.

2.3.3.1 Ion exchange by resin

Resins have a considerable influence on the adsorption of gold. Its adsorption technique was contemplated the most promising because of its fast adsorption speed, high loading capacity, low requirement on the clarity of solution, etc. (Dong et al., 2019). Moreover, ion exchange resins are the only economically practical method to concentrate and recover gold from such diluted media requires. Nevertheless, ion exchange resins still have some drawbacks: their application of gold recovery process from WEEE should be cautious since their preparation requires high costs that include the synthesis of a polymeric matrix and the selections of functional groups which can selectively remove gold (Cyganowski et al., 2017).

Purogold^{TM} products manufactured by Purolite Co. is the most prevalent commercial ion exchange resins for the recovery of gold, being functionalized by an admixture of a weak base and strong base amines (Balakrishnan & Ford, 1982). These functional group provided high adsorption capacity and selectivity towards gold. Nonetheless, the ion exchange resins must be applied in solutions after leaching of gold using immensely toxic cyanides. They are not appropriate for aqua regia systems since sharply basic quaternary amines deteriorate in the presence of nitric acid (Dorfner, 2011; Jermakowicz-Bartkowiak & Kolarz, 2013).

doi:10.6342/NTU202002980

2.3.3.2 Activated carbon adsorption

The application of activated carbon to recover gold from cyanide leach solutions in the last quarter of the 20th century affected the economics of gold ore processing. By replacing the Merrill–Crowe zinc cementation step, carbon-in-pulp (CIP) and carbon-in-leach (CIL) recovery provided a process that permitted the treatment of lower grade and disorderly ores (e.g., high-clay ores), at lower expense and operating costs and better metal recoveries (Staunton, 2016).

Recently, the thiosulfate system has extracted gold from carbonaceous ores, which shows that the gold–thiosulfate complex does not effectively adsorb onto activated carbon. This delivers carbon-in-pulp technology ineffective for the thiosulfate system. Early research also confirmed that activated carbon, which is in its original form does not adsorb the gold thiosulfate complex, perhaps due to the high anionic charge of the thiosulfate complex and the heaviness of the thiosulfate ions compared to gold cyanide (Yu et al., 2015).

Young et al. (2012) made activated carbon impregnated with cyano-cuprous species to recover the gold from thiosulfate solutions, which supposed that gold loadings as high as 2250 troy ounces per ton of carbon were noticed if the Au exchanged with Cu at a 1:1 ratio. Nevertheless, this is just theoretical, and the whole process still contains highly toxic cyanide, making it difficult to commercialize. Yu et al. (2015) manufactured AC impregnated with cupric ferrocyanide ($C_6Cu_2FeN_6$) species to recover the gold from the thiosulfate solution.

doi:10.6342/NTU202002980

Despite that, the full adsorption capacity was lessened, and the adsorption mechanism is not precise, which is not ideal for commercial applications.

Yu et al. (2018) made activated carbon impregnated with silver nitrate ($AgNO_3$), and potassium ferrocyanide ($K_4[Fe(CN)_6]\cdot 3H_2O$) to recover the gold from thiosulfate solution. The experiment results of adsorption predict that modified AC by $AgNO_3$ and $K_4[Fe(CN)_6]\cdot 3H_2O$ is a promising material to separate Au ions from $Au(S_2O_3)_2^{3-}$. In 100 mg L^{-1} gold solution at 50°C, the adsorption capability of $Au(S_2O_3)_2^{3-}$ is 3.55 kg t^{-1}, which is a significant property of the new AC.

Modified activated carbon with nitrogen and sulfur had an intense affinity for Au ion in the thiosulfate solution for the reason that the gold adsorption capacity attained about 25.85 kg t^{-1}. It was noticed that the adsorption of gold on the new AC might happen through a partial or complete ligand exchange reaction. In conclusion, modified activated carbon is regarded as the more competitive one to be used in ore pulp because of its higher hardness compared to resin (Chen et al., 2020).

doi:10.6342/NTU202002980

2.3.3.3 Electrometallurgical processes

The electrochemical progresses for gold recovery are fascinating as no extra chemical reagents are demanded, and the gold recovery can be precisely controlled by applying favorable process conditions. The electrochemical techniques boosted an interest in the extraction of noble metals from complex impure leaching solutions (Silva et al, 2019).

Lately, a method of silver recovery from zinc-containing solutions by means of cyclic electrodeposition-redox replacement (EDRR) (Halli et al., 2017). The EDRR process of gold recovery from the cupric chloride solution is schematically shown in Figure 2-3 (Korolev et al., 2018). It is composed of two subsequent steps: (1) The process introduces the inert working electrode into a solution containing both copper ions and gold ions. During the first step (Figure 2-3, B), copper ions lay on the electrode surface at constant cathodic potential E_{set}. (2) The cell remains in open circuit conditions until the prearranged cut-off potential E_{cut} reaches (Figure 2-3, C). The replacement of copper ions by gold ions can happen because the difference in their standard electrode potentials (Figure 2-3, D). These methods also can approach for gold recovery from cyanide-free solutions with only minor gold concentration (Korolev et al., 2018).

doi:10.6342/NTU202002980

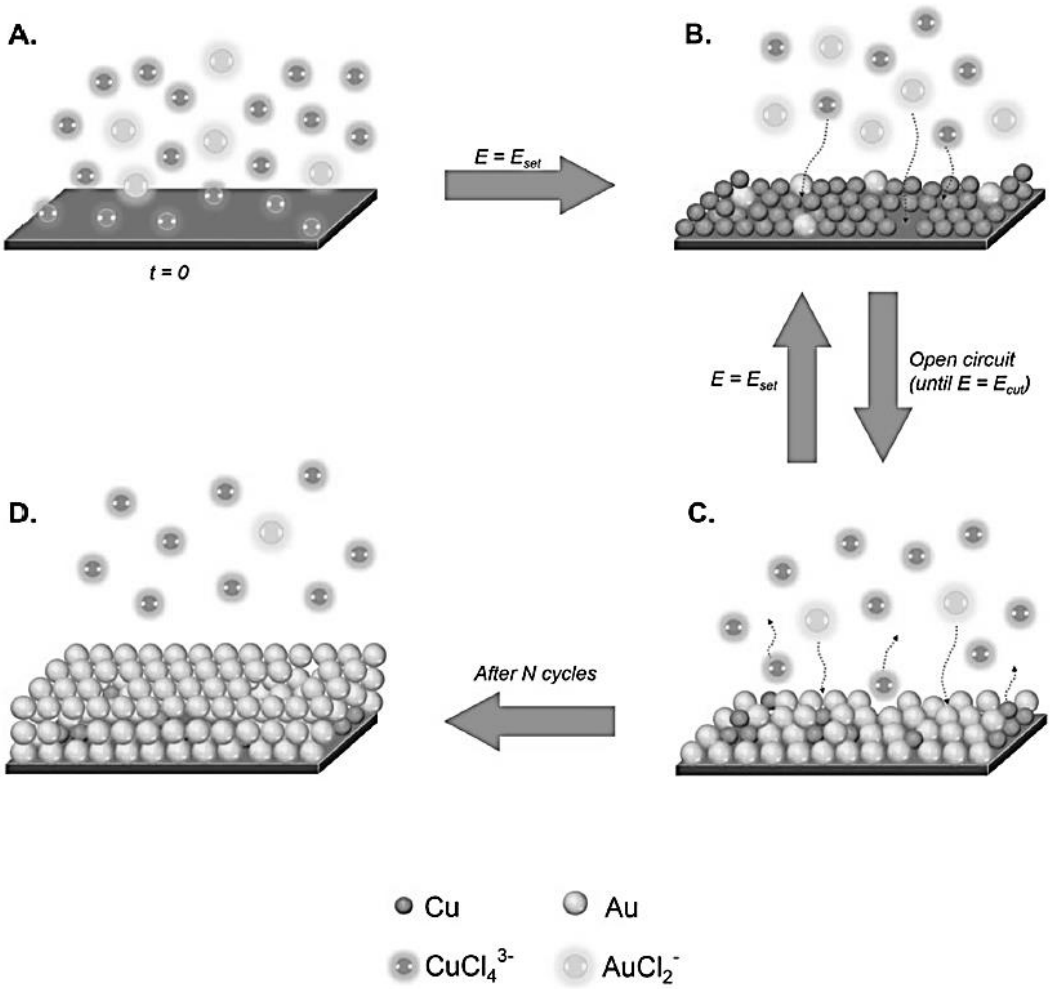

Figure 2-3 Mechanism of the electrodeposition-redox replacement (EDRR) cupric chloride solution (Korolev et al., 2018)

doi:10.6342/NTU202002980

2.3.3.4 Gold cementation

Gold can be leached using thiosulphate solution to form $Au(S_2O_3)_2^{3-}$. To reduce Au ion to Au element, Arima et al. (2002) claimed that gold-thiosulfate complex ion can be cementation by Zn, Cu, and Al powder because Zn, Cu, and Al had lower reduction potentials than Au. For Zn precipitation, the overall reaction of Au cementation is shown in Eqs. (2-4).

$$2Zn + 2[Au(S_2O_3)_2]^{3-} + 4NH_3 + 2H_2O \rightarrow [Zn(S_2O_3)_2]^{2-} + [Zn(NH_3)_4]^{2+} + 2S_2O_3)^{2-} + 2OH^- + H_2\uparrow + 2Au\downarrow \quad (2\text{-}4)$$

For Cu precipitation, the overall reaction of Au cementation is shown in Eqs. (2-5).

$$2Cu + 2[Au(S_2O_3)_2]^{3-} + 8NH_3 + 2H_2O + O2 \rightarrow [Cu(S_2O_3)_2]^{3-} + 2[Cu(NH_3)_4]^{2+} + 4OH^- + Au\downarrow \quad (2\text{-}5)$$

For Al precipitation, the overall reaction of Au cementation is shown in Eqs. (2-6).

$$3Al + 3[Au(S_2O_3)_2]^{3-} + 2NH_4OH + 6H_2O \rightarrow [Al(S_2O_3)_2]^- + 2(NH_4)[Al(OH)_4] + 4S_2O_3^{2-} + 3H_2\uparrow + 3Au\downarrow \quad (2\text{-}6)$$

doi:10.6342/NTU202002980

2.4 Activated Carbon

Activated carbons (ACs) are extremely porous carbonaceous materials that possess a distinct set of properties: a well-developed reproducible microporous structure, a high degree of surface reactivity, a major internal surface area, appreciable micropore volume, which can present a wide variety of pore size distributions (PSDs) and micropore size distributions (MPSDs) and an adsorption ability that makes them valid and adjustable adsorbents (White et al., 2013; Yu et al., 2018).

Chen et al. (2020) demonstrates that the large surface area, surface functional groups containing heteroatoms like oxygen, nitrogen, and sulfur influence the adsorption ability of activated carbon (Biniak et al., 1997; Macías-García et al., 1993). Furthermore, adsorption ability can also be influenced by hydrophobicity (Wu & Pendleton, 2001) and π-π interaction between aromatic organic materials and π electrons on activated carbon's graphene crystallite (Harris, Liu, & Suenaga, 2008).

2.4.1 Variety of Activated Carbon

Activated carbons aren't present in nature. The right selection of precursor and preparation process is vital for producing them. Several precursors, such as wood, coals, pitches, polymers, remains with a high amount of carbon, and different preparation methods have been used (White et al., 2013).

doi:10.6342/NTU202002980

There are different forms for activated carbons preparation, such as powders, granules, pellets, fibers, mesocarbon, microbeads, foams and aerogels, and flexible or rigid solids, shown in Figure 2-4 (Derbyshire et al., 2001). Owing to these characters and their distinct chemical properties, they can be used for very different applications, such as liquid- and gas-phase adsorption and energy storage.

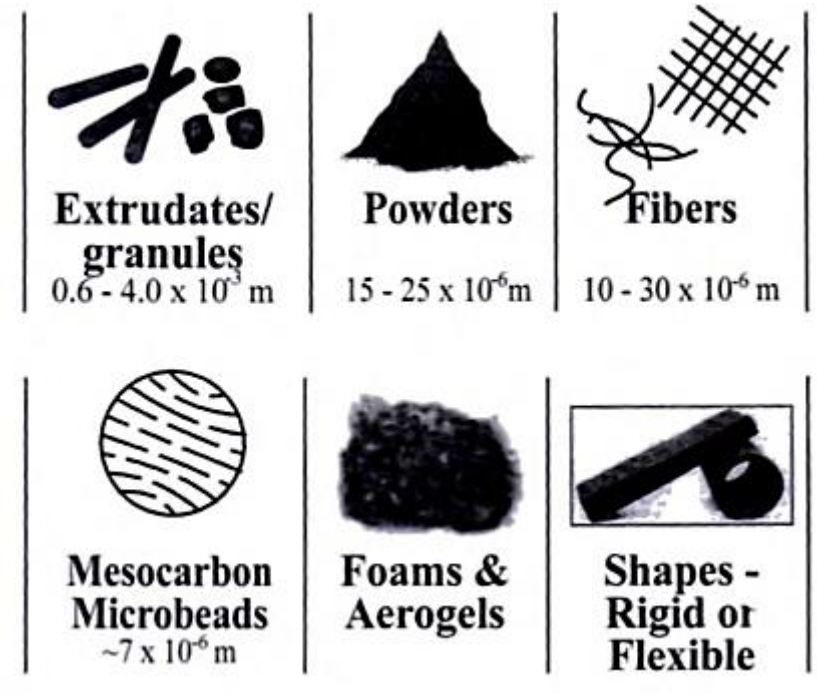

Figure 2-4 forms and properties of activated carbon (Derbyshire et al., 2001)

doi:10.6342/NTU202002980

2.4.2 Preparation of Activated Carbon Sphere (ACS)

Activated carbon spheres (ACS) are getting more attention because of their flexible size, porosity, and high surface area (Abbas et al., 2020).

The success of ACS in these applications strongly depends on the usability of ACS having cautiously controlled characteristics, for example, inner and outer diameters, and therefore controlled, surface properties, shell thickness, or textural properties such as mesoporosity of the carbon shell, and dispersibility in the relevant media. Much endeavor has been dedicated to the synthesis of ACSs by various approaches. The design and the synthesis of several types of ACSs through hard-templating, soft-templating, hydrothermal carbonization and activation by fluidized bed reactor are summarized below (Li et al., 2016).

2.4.2.1 Hard templating

In the hard-templating route, some specially prepared rigid particles are considered as "hard" core templates and sacrificed after the development of a carbon shell onto the core for constructing a hollow structure. The advantage of hard templates is having superior control of the product. However, getting rid of the template is extremely time consuming and is not environmentally friendly (Li et al., 2016).

Usually, the hardcore templates can be removed easily or not because of their chemical nature, calcination, dissolution, or etching after the constitution of carbon shells around the cores. The average inner diameter and diameter distribution of the resultant spheres are

doi:10.6342/NTU202002980

usually flexible depended on those of the hard templates applied. The typical hard-templating synthetic procedure for ACS is displayed in Figure 2-5: (1) coating of the template with the carbon precursor, (2) pyrolysis, and (3) elimination of the template. Various templates can be used, like silica spheres, polymer spheres, metallic spheres. (Kubo et al., 2010).

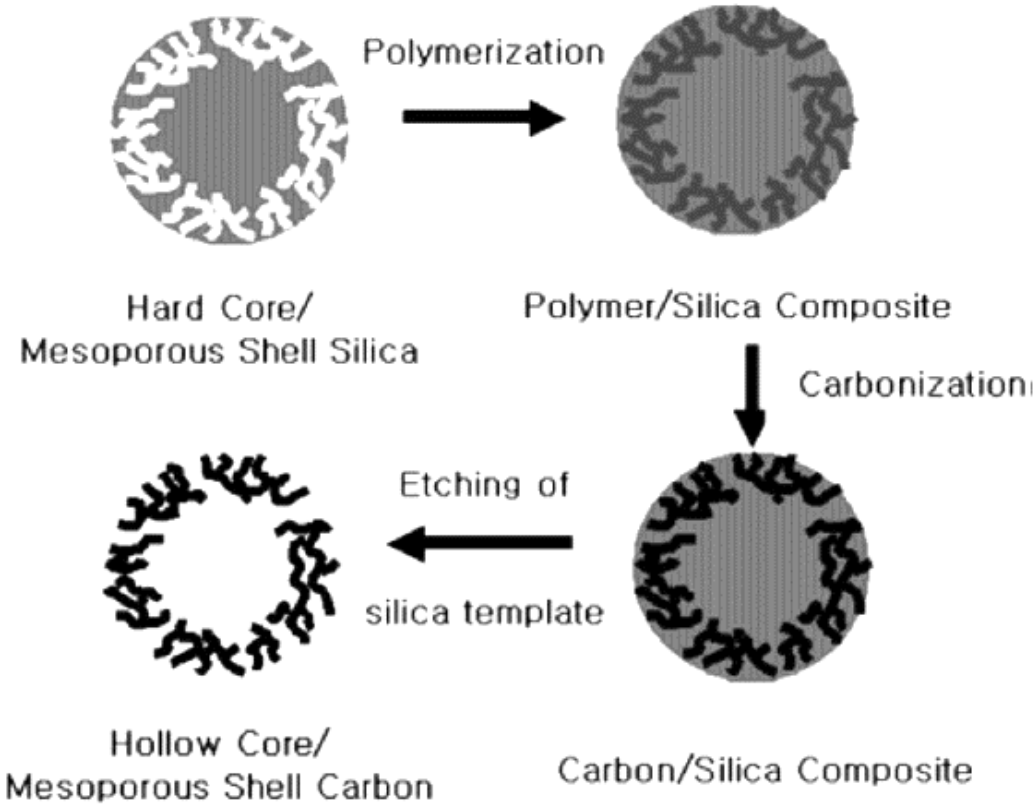

Figure 2-5 The hard-templating synthetic procedure (Li et al., 2016)

doi:10.6342/NTU202002980

2.4.2.2 Soft templating

The soft-templating method indicates that the hollow structure generates by self-assembly of carbon precursors and other organic compounds having a structuration function (Li et al., 2016). The core templates are usually “soft” precursor molecules, surfactants, or some organic additives, which will decompose during the pyrolysis forming ACS (Li & Shi, 2014). The soft template is rather easy to eliminate compared to the hard template; however, the morphology of the target products is difficult to control (Li et al., 2016).

Emulsion droplets, micelles, vesicles, or gas bubbles can be colloidal systems, which usually originate from precursor molecules or from some additives originally added for building the hollow structures. Despite such advantages, the morphology and the monodisperse character of the as-prepared hollow products are less satisfactory than those with hard-templating due to the polydispersity and the dynamics of soft templates (Li et al., 2016).

doi:10.6342/NTU202002980

2.4.2.3 Hydrothermal carbonization

Ever since their first synthesis by Friedrich Bergius, tremendous attention has been received by hydrothermal carbonization (HTC) as a sustainable synthetic method to produce carbon spheres (CSs) (Hekmat et al., 2020)

Hydrothermally carbonized is formed of the heat treatment of organic solution such as saccharides (cellulose, glucose, starch, or sucrose), furfural, or more complex substances like biomass, at temperatures between 130°C and 250°C under autogenous pressure (Zhu et al., 2010). There are three benefits in this procedure: (1) the precursors are readily available, cheap, and renewable (i.e., saccharides or biomass), (2) it is a eco-friendly and uncomplicated process because it only comprises water as the solvent with simple heat treatment in a closed autoclave, and (3) the resulting solid carbon materials exhibit superior chemical and structural properties, as well as an absolutely high content of oxygen-containing functional groups (Khanra et al., 2012). The quantities and species of these functional groups can be arranged by altering the operating conditions, including temperature, solution concentration, reaction time, and precursor.

In recent years, HTC has demonstrated its capability of transforming biomass to carbon materials through very mild processing conditions (Fan et al., 2011). Its full potential as a synthetic method for carbon materials that have prospective applications in several fields

doi:10.6342/NTU202002980

such as energy storage, catalysis, water purification, CO_2 sequestration, and agriculture has only been completely understood in the last decade (Sui et al., 2011).

2.4.2.4 Physical Activation and Chemical Activation

There are two processes to produce activated carbons, including physical activation and chemical activation. Physical activation is the most ordinary activated carbon production process. This process can separate into two-stage: (1) carbonization, the precursor material is pyrolyzed in an inert gas such as nitrogen at a medium-high temperature (300-800°C). During carbonization, the volatile fraction of the precursor material releases. The initial porosity after carbonization has a low adsorption capacity because mostly tars released and block the pores. (2) activation, the purpose of the activation stage is required to enlarge the existing porosity and enhance the adsorption capacity (Pallarés, González-Cencerrado, & Arauzo, 2018). During the activation stage, char is activated at a higher temperature (700–1000°C) in the presence of an activating gas, like steam, CO_2, and air. Throughout this process, the carbonaceous matrix undergoes several heterogeneous reforming reactions resulting in a sizeable porous structure and increasing its specific surface area. After activation, more mesopores and macropores developed, and the BET surface area and pore volume reduce with an increased activation time (Zhang et al., 2014).

doi:10.6342/NTU202002980

In the chemical activation process, the precursor is impregnated with activating chemical agents such as KOH, H_3PO_4, or $ZnCl_2$. Later, the precursor is dealt with a carbonization process at medium temperatures about 550°C. Eventually, the resulting activated carbon is washed to remove chemical agents. However, physical activation is preferred at an industrial scale, since it allows for the optimization of microporosity, reducing both the process' costs and associated pollution (Pallarés et al., 2018).

The vertical tubular furnace is an equipment to make the materials fluidized in physical activation. The fluidized bed reactor provides the advantage of extraordinarily high heat and mass transfer. It gives better activation in less time and at a lower temperature compared to the static bed process (Kirubakaran et al., 1991). In the fluidized bed reactor, not only are the activating gases immediately brought in to connect with the raw material, but the waste gases are also just as quickly removed while revealing the fluidizing activated carbon to fresh incoming gas (Kunii & Levenspiel, 1969). Figure 2-6 shows the schematic diagram of the fluidized bed reactor.

doi:10.6342/NTU202002980

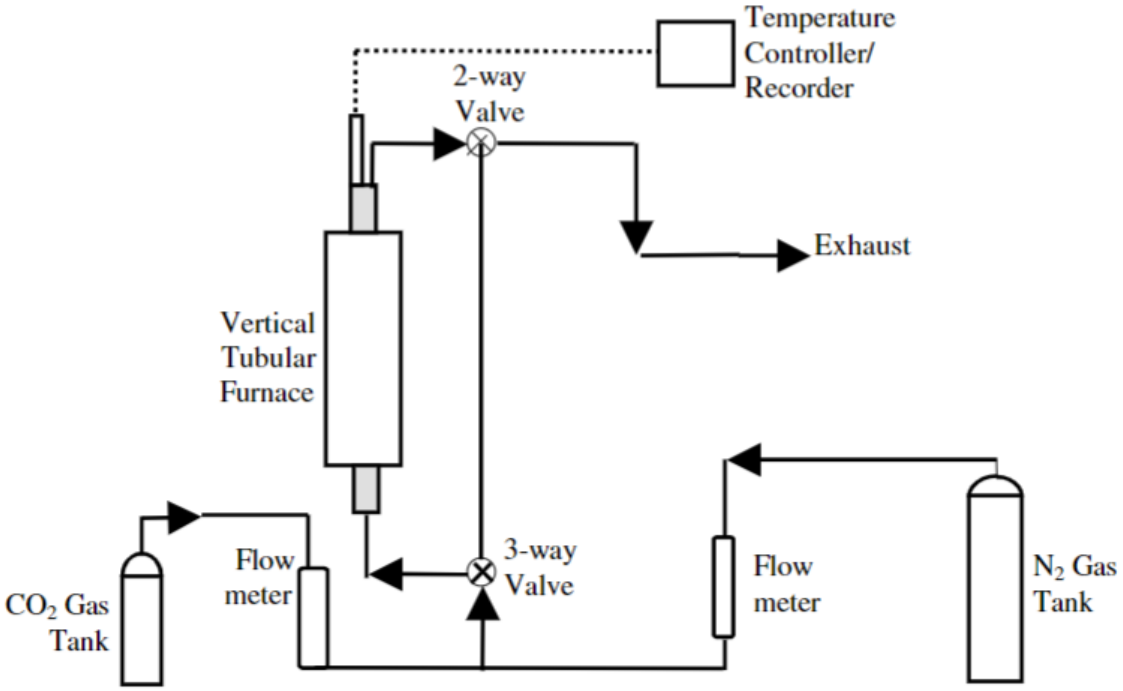

Figure 2-6 Schematic of the fluidized bed reactor setup (Daud & Ali, 2004)

2.4.3 Applications of AC

Because of the discovery of fullerenes, carbon nanotubes, and graphene, valuable carbon materials has been studied a lot. Their potential applications are carbon fixation, catalyst supports, adsorbents, gas storage, electrodes, fuel cells and stationary phases in liquid chromatography (Li et al., 2016; Titirici, Thomas, & Antonietti, 2007).

2.5 Adsorption

The definition of adsorption is the net accumulation of a chemical species at the interface between a solid phase and an aqueous solution phase (Sposito, 1989). In adsorption this accumulation is limited to a two-dimensional molecular structure on the surface. the

doi:10.6342/NTU202002980

surface where the accumulation occur is called the adsorbent, and the chemical species that accumulates at the interface is called the adsorbate (Goldberg, 2015).

2.5.1 Langmuir isotherm

Numerous theoretical explanations generate adsorption isotherms. The simplest theoretical model that can be used to illustrated monolayer adsorption is the Langmuir equation (Meghea, et al., 1998). The Langmuir equation is based on a kinetic approach and assumes a uniform surface, a single layer of adsorbed material, and constant temperature. This model is beneficial when there is a robust concrete interaction between the surface and the adsorbate so that a single adsorbed layer forms and no multi-layer adsorption happens. The types of Langmuir isotherm are presented by the following equations (2-7) and (2-8):

$$q_e = \frac{Q_m K_L C_e}{1+K_L C_e} \tag{2-7}$$

$$\frac{C_e}{q_e} = \frac{1}{Q_m K_L} + \frac{C_e}{Q_m} \tag{2-8}$$

where C_e is the equilibrium concentration (mg/L), q_e is the adsorption capacity in equilibrium (mg/g), K_L is the Langmuir adsorption constant (L/mg), and Q_m is the theoretical maximum adsorption capacity (mg/g). The essential characteristics of the Langmuir isotherm can be expressed in terms of a dimensionless constant separation factor S_F that is given by the equation (2-9):

doi:10.6342/NTU202002980

$$S_F = \frac{1}{1+C_0 K_L} \quad (2\text{-}9)$$

where C_0 is initial concentration of adsorbate. For favorable sorption, $0 < S_F < 1$; for unfavorable sorption, $S_F > 1$; for linear sorption, $S_F = 1$; for irreversible sorption, $S_F = 0$ (Can et al., 2016).

2.5.2 Freundlich isotherm

The Freundlich isotherm is appropriate for use with heterogeneous surfaces but merely describe adsorption data over a restricted range. It is often found that when the Freundlich equation is fitted to data at high and intermediate concentrations. Typically, activated carbons have isotherms that obey the Freundlich model in the middle range of pressure, with less agreement at high pressures and low temperatures (Ng et al., 2002). The Freundlich adsorption isotherm can be expressed in the equations (2-10) and (2-11):

$$q_e = K_F C_e^{\frac{1}{n}} \quad (2\text{-}10)$$

$$\log q_e = \log K_F + \frac{1}{n} \log C_e \quad (2\text{-}11)$$

where K_F (L/mg) and n are isotherm constants represent the capacity and heterogeneity factor of the adsorption, respectively. When 1/n is >1, the change in adsorbed concentration is greater than the change in the solute concentration.

doi:10.6342/NTU202002980

2.5.3 Temkin isotherm

Temkin isotherm explicitly explained the adsorbent-adsorbate interactions. The model assumes that heat of adsorption of all molecules in the layer would decrease linearly rather than logarithmic with coverage by ignoring the extremely low and large value of concentrations, (Johnson & Arnold, 1995). The Temkin adsorption isotherm assumes that heat of adsorption decreases linearly with the sorption coverage (Can et al., 2016). The Temkin adsorption isotherm can be expressed in the equations (2-12) (Pathania et al., 2017; Wang & Qin, 2005):

$$q_e = \beta ln a + \beta ln C_e \quad (2\text{-}12)$$

where $\beta = \frac{RT}{b}$, R is the general gas constant (8.314 $Jmol^{-1}$ K^{-1}), T is absolute temperature (K), a and bare the Temkin isotherm constants, and b (J mg^{-1}) is related to heat of sorpion.

doi:10.6342/NTU202002980

Chapter 3 Materials and Methods

3.1 Research framework

A flowchart of the research framework is given in Figure 3-1, which is composed of three parts. The first part is the preparation of the material, in which ACS is activated by a fluidized bed reactor and TUACS is synthesized by adding ACS into the thiourea solution. The second part is chemical and physical characterization, where ACS and TUACS are analyzed by elemental analysis (EA), X-ray diffraction (XRD), X-ray photoelectron spectroscopy (XPS), scanning electron microscopy/energy-dispersive X-ray spectroscopy (SEM/EDS), transmission electron microscopy (TEM), Brunauer-Emmett-Teller (BET) method based on N_2 adsorption, and Raman spectroscopy (Raman). The last part is the adsorption, desorption, and regeneration experiments, in which the operating variables include pH value, time, and dosage. The optimal conditions were found, in order to carry out subsequent isotherm and selection experiments. The purpose of the desorption experiments was to understand the leaching agent ($(NH_4)_2S_2O_3$) on the effectiveness of reuse and recovery of Au. To determine if TUACS is reusable, repeated adsorption and desorption experiments were performed.

doi:10.6342/NTU202002980

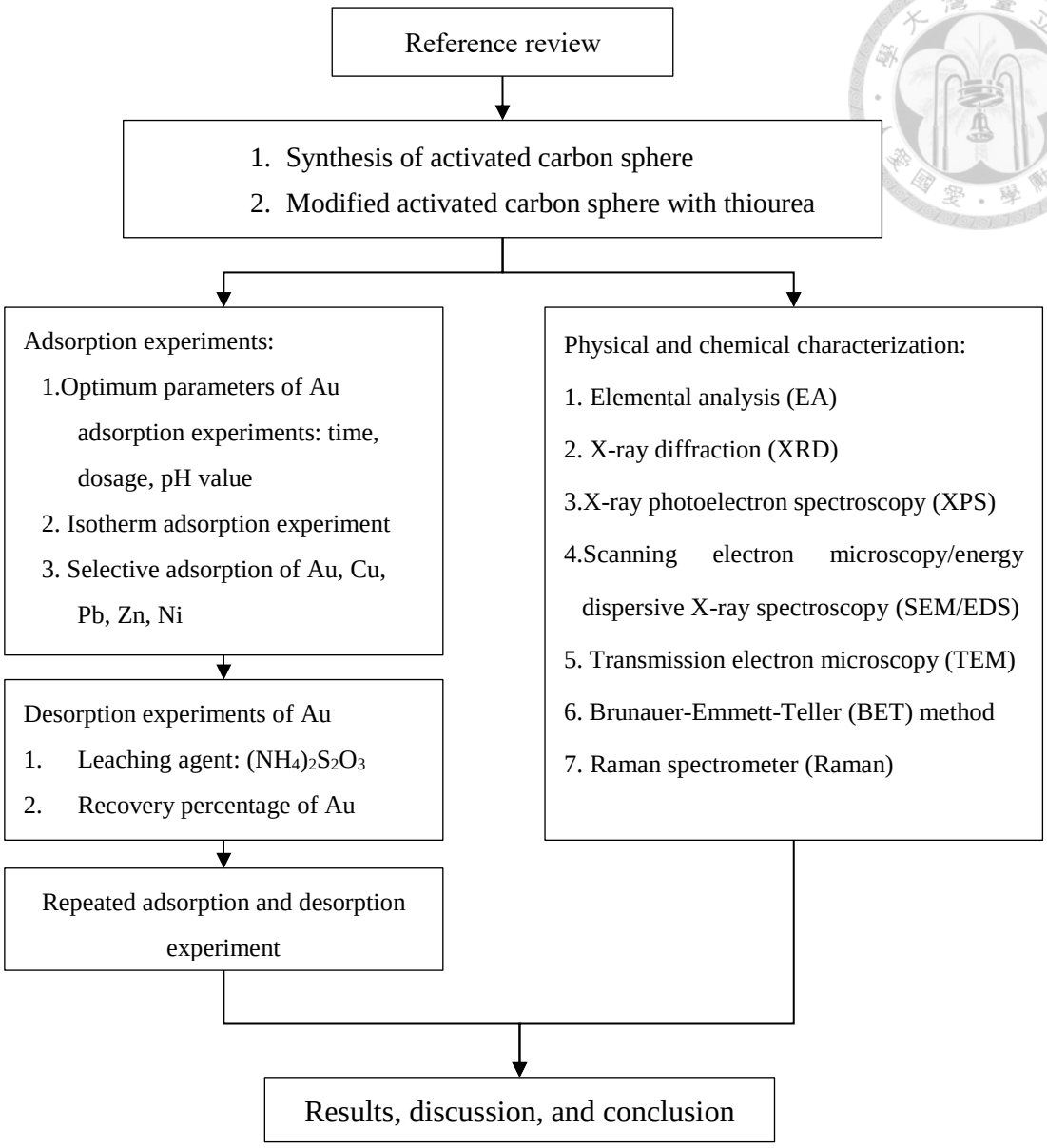

Figure 3-1 The flowchart of research framework

doi:10.6342/NTU202002980

3.2 Preparation of activated carbon sphere (ACS)

Commercially obtained phenol-formaldehyde (PF) resin spheres were carbonized at 500°C for 1 h to remove most of the volatile contents from the spheres and reorganize the carbon structure. The carbonized spheres were then further developed for increasing porosity by physical activation. 3 g of the carbonized PF spheres were added into a cylindrical quartz tube reactor. The activation temperature was set at 900°C, the activation time was 4 h, and carbon dioxide (CO_2, 99.999%) was used to activate the ACS. As shown in Figure 3-2, the activation process was conducted in a fluidized bed reactor comprising of a conventional temperature-programmed furnace mounted vertically and a cylindrical quartz tube with an inner diameter of 20 mm in the middle of the furnace. The cylindrical quartz tube was sealed at the both ends of the tube with quartz plugs, ensuring the spheres to blow out of fall down from the ends and a gas-tight environment in the reaction chamber during activation. The fluidized bed reactor was purged with high purity nitrogen (N_2, 99.999%) and heated to 900°C. After achieving a temperature of 900°C, the gas was then changed from N_2 to CO_2 for activation. The flow rate of N_2 and CO_2 was controlled at 150 mL min^{-1} by a rotameter. The temperature was set to rise at 10°C min^{-1}. The actual photo for vertical tubular furnace, quartz tube, and temperature controller are shown in Figure 3-3.

doi:10.6342/NTU202002980

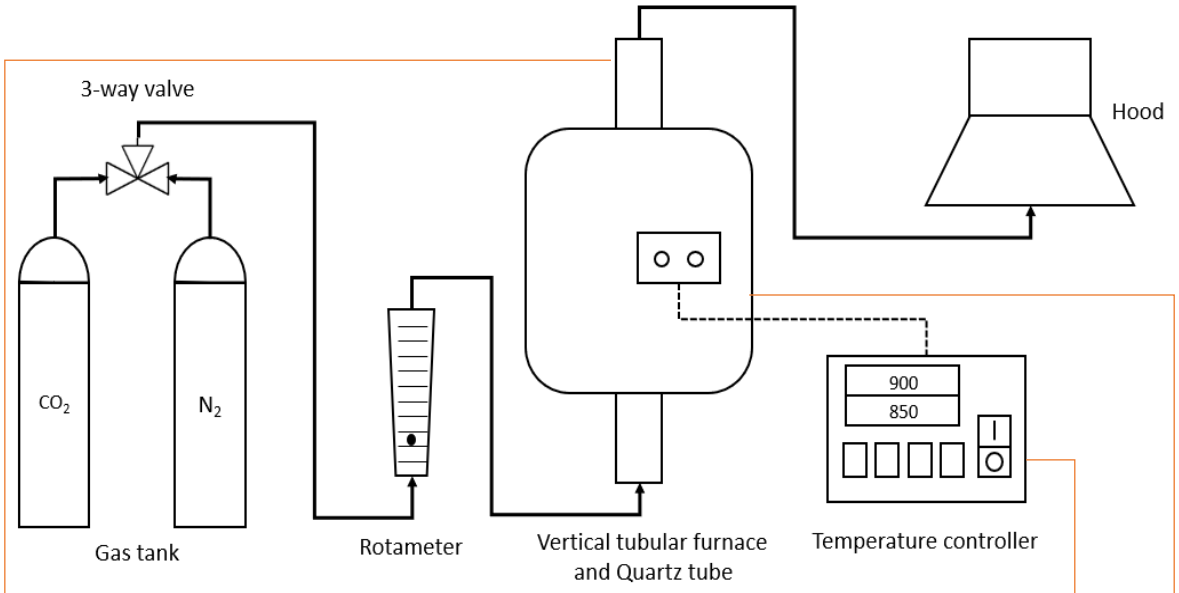

Figure 3-2 Fluidized bed reactor system for preparing ACS

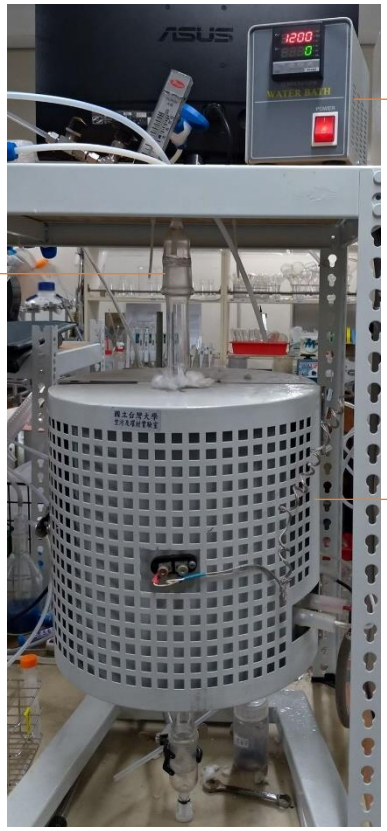

Figure 3-3 The photo of the vertical tubular furnace, quartz tube, and temperature controller

doi:10.6342/NTU202002980

3.3 Preparation of modified activated carbon sphere by thiourea (TUACS)

Figure 3-4 illustrates the preparation steps for TUACS. The synthesized method for TUACS is referred to previous studies (Chen et al., 2020; Song et al., 2019; Wang et al, 2018). The solution used for activated carbon modification was prepared by mixing 3 g of thiourea (TU) with 50 mL of ethanol (EtOH) and 100 mL of deionized (DI) water. After the TU solution was completely dissolved in the beaker, 0.5 g of ACS was added into the beaker. Afterwards, the beaker was placed on a hot plate stirrer and stirred at 60°C for 8 h. After 8 h, the TUACS was washed with EtOH and DI water once and three times, respectively, by centrifuge and subsequent filtration. Lastly, the TUACS was dried at 50°C for 24 h in the drying oven.

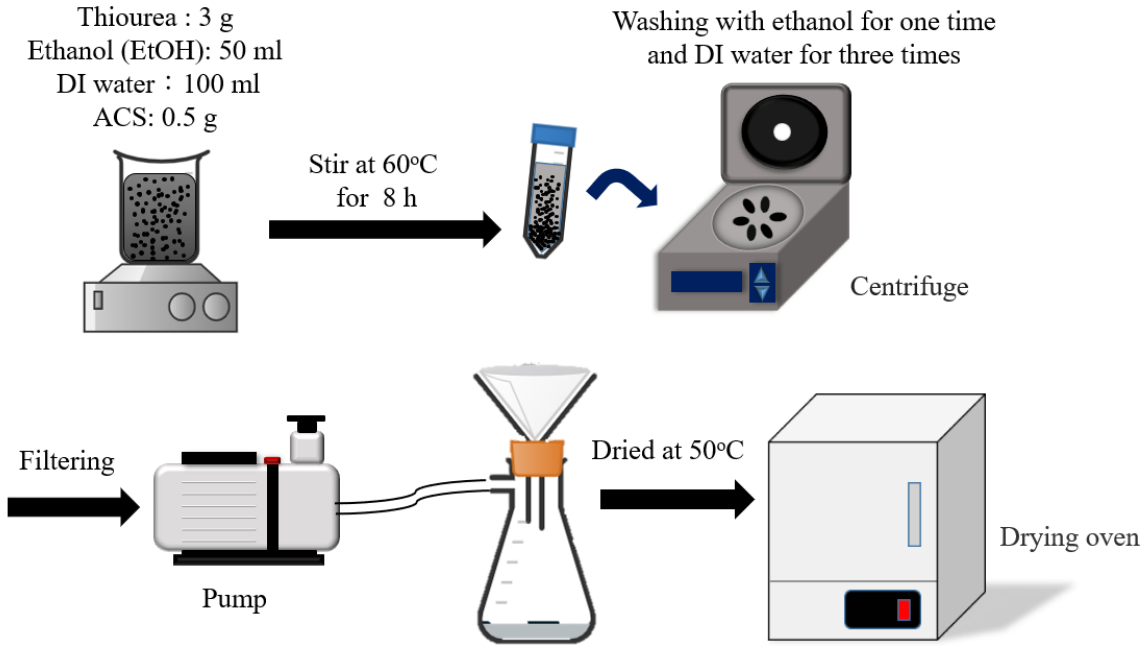

Figure 3-4 the preparation steps of TUACS

doi:10.6342/NTU202002980

3.4 Analytical instruments, experimental equipment, experimental reagents

Table 3-1 presents the instruments for physical and chemical characterization used in this study.

Table 3-1 Instruments for physical and chemical characterization

Analysis item	**Manufacturer**	**Model**
Elemental analysis	Elementar	Vario EL cube
X-ray Diffraction	Bruker	D2 Phaser
X-ray Photoelectron spectroscopy	VG	Scientific ESCALAB 250
Scanning Electron Microscopy/ Energy dispersive X-ray spectroscopy	JEOL/ OXFORD	JSM-7600F/ X-MaxN TSR
Transmission Electron Microscopy	Hitachi	H-7100
Specific surface area, pore volume, and pore size distribution (PSD)	Micromeritics	ASAP2420
Raman Spectrometer	Thermo	Nicolet Almega XR
Inductively Couple Plasma Optical Emission Spectrometry	Agilent	700 Series

doi:10.6342/NTU202002980

3.4.1 Elemental analysis (EA)

Elemental analysis evaluates the weight percentage of elements, including carbon (C), hydrogen (H), nitrogen (N), oxygen (O), and sulfur (S) in a compound. The analytical method consisted of injecting a capsule into a high temperature furnace and combusting it with pure oxygen. Excess oxygen is added to ensure total combustion of all inorganic and organic substances by the end of the combustion period. The resulting combustion products pass through specialized reagents to produce carbon dioxide (CO_2), water (H_2O), nitrogen (N_2), nitrogen oxides (NO_x), and sulfur oxides (SO_x). Then, the gases are passed over copper to reduce nitrogen oxides to N_2. After scrubbing, the gases enter a mixing volume chamber to ensure homogeneous mixing. The mixture then passes through the thermal conductivity detectors (TCD) for each individual gas, for which each TCD includes a pair of thermal conductivity cells. The percentage of C, H, N, and S in the compound was analyzed for CO_2, H_2O, NO_x and SOx content, respectively. In addition, the compound was pyrolyzed to produce CO_2 and CO for analysis of O content by TCD.

3.4.2 X-ray diffraction (XRD)

The crystal phase was identified by measurement using X-ray diffraction with CuKα radiation (λ=1.5405Å). The material was scanned continuously from $2\theta = 10^o$ to $2\theta = 90^o$ with a 0.03^o step size and a counting time of 4 s/step. The phases of crystalline were identified using the JCPDS (Joint Committee on Powder Diffraction Standards) database.

doi:10.6342/NTU202002980

3.4.3 X-ray photoelectron spectroscopy (XPS)

X-ray photoelectron spectroscopy was used to measure the surface chemical composition of ACS and TUACS. The XPS spectra were acquired by irradiating the material with a beam of X-rays while measuring the binding energy simultaneously. To remove impurities, the samples were dried at 105°C for 24 h. Next, the samples were scanned by the Alκα-ray at 400 W and 15 kV. The peaks of the XPS spectra could be adopted to decide which types of functional groups exist on the surface of ACS and TUACS.

3.4.4 Scanning electron microscopy/energy dispersive X-ray spectroscopy (SEM/EDS)

SEM is an instrument for which the electrons interact with the atoms that constitute the sample, producing signals that yield a high-resolution image of surfaces. EDS is an analytical technique used for the elemental analysis of a sample. The fundamental principle of EDS is that each element has a unique atomic structure allowing the X-rays to be released due to a difference in energy after electron excitation. The ACS and TUACS were dried at 105°C for 24 h and then characterized for morphology and elemental analysis by SEM/EDS. The signal would be converted into morphology at 10 kV.

3.4.5 Transmission electron microscopy (TEM)

TEM can be used to observe properties such as crystal structure and other features within the structure. The basic principle of TEM involves a high energy beam (around 100kV-1MV) of electrons that is shone through a sample, and the interactions between the

doi:10.6342/NTU202002980

electrons. The lighter areas of a TEM image represent those areas of the sample where more electrons were transmitted through, whereas the darker areas of a TEM image indicate that fewer electrons were transmitted through the sample at that point. ACS and TUACS were ground and washed with ethanol solution, then visualized by the TEM instrument.

3.4.6 Specific surface area, pore volume, and pore size distribution (PSD)

The specific surface area (S_{total}) was calculated by the Brunauer-Emmett-Teller (BET) theory, which illustrates the physical adsorption of gas molecules onto a solid surface. The BET theory generally utilizes probing gases that do not chemically react with material surfaces like nitrogen (N_2) as a gaseous adsorbate. In this regard, standard BET analysis is most often conducted at the boiling temperature of N_2 (77 K). The micropore surface area (S_{micro}) and micropore volume (V_{micro}) were obtained via a t-plot method. In this method, the adsorbed amount is expressed by the thickness of the adsorption layer, t. The total pore volume (V_{total}) was calculated at $P/P_0 = 0.995$. The pore size distribution (PSD) curve was calculated from the Barrett, Joyner, and Halenda (BJH) desorption isotherm, as well as the non-localized density functional theory (NLDFT). The BJH method was used to calculate the mesopore distribution, while NLDFT estimated the micropore distribution. During this operation, ACS was degassed at 200ºC for 17 h, while TUACS was degassed at 90ºC. The N_2 adsorption measurement occurred between 10^{-3} and 0.995 of the standard pressure at 77 K.

doi:10.6342/NTU202002980

3.4.7 Raman spectroscopy

Raman spectroscopy obtains information regarding elucidating structure, composition, coordination, and bonding of sample molecules by changes in energies of scattered monochromatic radiations (Krishna, Unsworth, & Edge, 2016). The ACS and TUACS were ground and put onto glass slides and covered with coverslips for observation of the structure by Raman spectrometer with a 532 nm laser excitation, and ×10 working distance objectives.

3.4.8 Inductively couple plasma optical emission spectrometry (ICP-OES)

Inductively Couple Plasma Optical Emission Spectrometry was conducted to detect the concentration of metal components. The metal ion solution was injected into the chamber and sprayed to form an aerosol. Then, the aerosol was transited to the torch, which has a high temperature plasma of 7000 to 10000 K. The aerosol, including the metal elements, was excited to an atomized state. When the excited atoms returned to their lower energy positions, emission rays were released. The metal concentration is determined based on the photon rays' intensities through the photosensitive device.

doi:10.6342/NTU202002980

3.4.9 Experimental equipment

The experimental reagents used in this research are shown in Table 3-2.

Table 3-2 experimental equipment

Equipment	Manufacturer	Model
Reciprocate shake water bath	Chemist	DKW-40
Water purification system	Millipore	Milli-Q
Ultrasonic cleaner	GT sonic	GT-2200QTS
pH meter	SUNTEX	SP-2300
Centrifuge	Thermo scientific	Heraeus Megafuge 16
Filter paper	ADVANTEC	Ø 1 μm
Glass bottle	-	110 mL

doi:10.6342/NTU202002980

3.4.10 experimental reagents

The experimental reagents used in this research are summarized in Table 3-3

Table 3-3 Experimental reagents

Chemicals	Manufacturer	Properties
phenol-formaldehyde resin spheres	-	Reagent grade
Thiourea	Sigma-Aldrich	99%
Ethanol	Honeywell	99.8%
Copper (Ⅱ) nitrate	SHOWA	98%
Lead nitrate	J.T. Baker	99.8%
Zinc nitrate	Alfa Aesar	99%
Nickel (Ⅱ) nitrate	Alfa Aesar	99.9%
Ammonium thiosulfate	Alfa Aesar	96%
Hydrochloric acid	J.T. Baker	36.5-38%
Nitric acid	J.T. Baker	69.0-70.0%
Gold ICP standard	AccuStandard	1000 μg mL^{-1}
Multi-element ICP standard	AccuStandard	1000 μg mL^{-1}

doi:10.6342/NTU202002980

3.5 Adsorption experiments of Au by TUACS

For the purpose of understanding the characterization of Au adsorption by TUACS, a series of experiments was conducted to evaluate the effect of variables including time, TUACS dosage, and pH value. Additionally, Langmuir and Freundlich isotherms were used to analyze the equilibrium data. The Au ion solution was prepared by an Au ICP standard. A variable dosage of TUACS was placed into a 50 mL Au ion solution. Then, the solution with TUACS was shaken in a reciprocal shaking water bath at 30°C, and the speed was set to 150 rpm for several hours. The dosages of TUACS were 0.01, 0.02, 0.03, 0.04, 0.05, 0.06, and 0.07 g L^{-1}. The pH values of the solution were adjusted to 0.5, 2, 4, 6, 8, and 10. The contact time was controlled at 12, 24, 48, 72, 96, and 120 h. For the adsorption isotherm experiments, the initial concentration of Au was 10, 20, 30, 40, and 50 mg L^{-1}. After adsorption, the solution was filtered by 1 μm diameter filter paper. The filtered Au solution was then analyzed by ICP-OES. The method detection limit (MDL) of Au was 4.3 μg L^{-1}. The removal efficiency of Au was calculated by equation (3-1):

$$\text{Removal efficiency (\%)} = \frac{C_0 - C_t}{C_0} \times 100\% \quad (3\text{-}1)$$

where C_0 (mg L^{-1}) is the initial Au concentration and C_t (mg L^{-1}) is the residual Au concentration after adsorption experiments.

The Au adsorption capacity of TUACS, which is an index to measure the Au adsorption ability of the adsorbent, was calculated by equation (3-2):

doi:10.6342/NTU202002980

$$q = \frac{(C_0 - C_t) \times V}{M} \quad (3\text{-}2)$$

where q (mg/g) represents the Au capacity of sorbent, V (L) represents the volume of the Au solution, and M (g) represents the weight of TUACS used in the adsorption process. In addition, Langmuir and Freundlich isotherms were calculated by equation (2-5) and (2-8).

3.6 Selective adsorption experiments of Cu, Pb, Zn, Ni, and Au by carbonized PF resin sphere and TUACS

The selective adsorption experiments were conducted in a mixed solution containing Cu, Zn, Ni, and Pb ions. The solution's pH was controlled at 2.0, and the contact time was 96 h in a reciprocal shaking water bath at 30°C and 150 rpm. The Cu, Pb, Zn, and Ni ion solution was prepared by dissolving copper nitrate, lead nitrate, zinc nitrate, and nickel nitrate. The method detection limit (MDL) of Cu was 2 μg L^{-1}, Pb was 11 μg L^{-1}, Zn was 1 μg L^{-1}, and Ni was 1 μg L^{-1}. To compare the selective adsorption efficiency of carbonized PF resin spheres and TUACS, selective adsorption experiments were conducted. The initial concentration of the gold ion solution was 10 mg L^{-1}. Moreover, in order to simulate metal concentrations found in the wastewater of PCBs, the Cu concentration was set at 100 mg L^{-1}, the Pb, Zn, and Ni concentrations were 20 mg L^{-1}, and the concentration of Au was 0.01 mg L^{-1}. Selective adsorption for Au = 0.01 mg L^{-1}, which is a low concentration of Au, was only carried out by TUACS. The concentration of metals before and after adsorption were measured by ICP-OES.

doi:10.6342/NTU202002980

3.7 Desorption experiments of Au

It is essential to strip gold from TUACS because Au could be refined to pure gold or the stripping Au solution could be further used as the plating solution. In this research, we used the ammonium thiosulfate ($(NH_4)_2S_2O_3$) as the leaching agent since ammonium thiosulfate is environmentally friendly for Au extraction. The dosage of TUACS-Au was 0.06 g L^{-1}. The concentrations of ammonium thiosulfate were 0.1, 0.2, 0.3 and 0.4 M. The solution of ammonium thiosulfate was placed into the glass bottle with TUACS after adsorbing the Au (i.e., TUACS-Au). 50 mL of different concentration of ammonium thiosulfate solution with TUACS-AU was shaken in a reciprocate shake water bath at 150 rpm of rotating speed and a 30°C. After the desorption experiments, the solution was filtered by filter paper. The filtered solution of Au was analyzed by ICP-OES. Desorption efficiency of Au is calculated by equation (3-3):

$$\text{Desorption efficiency (\%)} = \frac{M_0 - M_t}{M_0} \times 100\% \qquad (3\text{-}3)$$

where M_0 (mg g^{-1}) is the gold capacity of TUACS before stripping and M_t (mg g^{-1}) is the gold capacity of TUACS after stripping.

doi:10.6342/NTU202002980

3.8 Repeated adsorption and desorption experiments of Au

For understanding the reusability of TUACS, the repeated adsorption and desorption experiments of Au were conducted. The artificial wastewater was prepared by Au ICP standard. The solution of the initial concentration of Au was 10 mg L^{-1}. 0.06 g L^{-1} of TUACS was added into 50 mL Au solution. The solution with TUACS was shaken in a reciprocate shake water bath for 96 h at pH 2, 150 rpm of rotating speed and at 30^{o}C. After the experiments, the solution was filtered by filter paper. For desorption experiments, the solid of TUACS after adsorption was added to 50 mL of ammonium thiosulfate solution. The experiment of adsorption and desorption was repeated for five times. The remained Au concentrations were then analyzed by ICP-OES.

doi:10.6342/NTU202002980

Chapter 4 Results and Discussion

4.1 Physical and chemical characterization of ACS and TUACS

4.1.1 Elemental analysis (EA)

Table 4-1 presents the elemental analysis, including carbon (C), nitrogen (N), sulfur (S), oxygen (O), and hydrogen (H) contents of carbonized PF sphere, ACS, and TUACS. After activation, the carbon and sulfur contents of ACS were 91.3% and 0.128% respectively, while the carbon and sulfur contents of TUACS decreased by nearly 10% and grew to 10.7%, respectively. This result indicated the ACS was successfully modified with thiourea, resulting in a noticeable sulfur content increase. The nitrogen contents did not change, which may be due to the decomposition of thiourea into the NH_3 gas (Wang et al., 2017).

Table 4-1 Element analysis of ACS and TUACS

	C (%)	H (%)	N (%)	S (%)	O (%)
Carbonized PF sphere	85.1	3.63	1.53	2.94	6.80
ACS	91.3	1.49	1.38	0.13	4.66
TUACS	80.1	2.74	1.82	10.7	7.04

doi:10.6342/NTU202002980

4.1.2 Scanning Electron Microscopy/ Energy dispersive X-ray spectroscopy (SEM/EDS)

To characterize the morphology and elements, ACS and TUACS were analyzed by SEM/EDS. Figure 4-1 shows the photo of ACS, and Figure 4-2 displays SEM images for four different levels of magnification for ACS. The highest magnification was x50000 in Figure 4-2 (iv), indicated that ACS had a rough surface and there were some large transit pores shown in the image, with a size approximately at 2.5 μm, and numerous small mesopores with sizes <0.05 μm. To observe the structure inside the ACS more distinctly, the ACS was ground and subsequently analyzed by SEM. As shown in Figure 4-3, the pores inside the ACS were widespread and unevenly distributed with various sizes, suggesting the complex porous structure of ACS.

As observed in Figure 4-4, the SEM image of TUACS was comparable to the SEM image of ACS, therefore TUACS was further analyzed by EDX. Figure 4-4 (iii) illustrates that TUACS contained the elements C, O and S. After adsorption experiments with 10 mg L^{-1}Au, the TUACS-Au was ground and analyzed by SEM/EDX, and the photo of TUACS-Au is shown in Figure 4-5. The mapping image was given in Figure 4-6. In Figure 4-6(iii), it was observed that S was randomly distributed inside the TUACS-Au, while the Au was almost entirely distributed on the surface of the TUACS-Au in Figure 4-6(iv).

doi:10.6342/NTU202002980

Figure 4-1 The photo of ACS

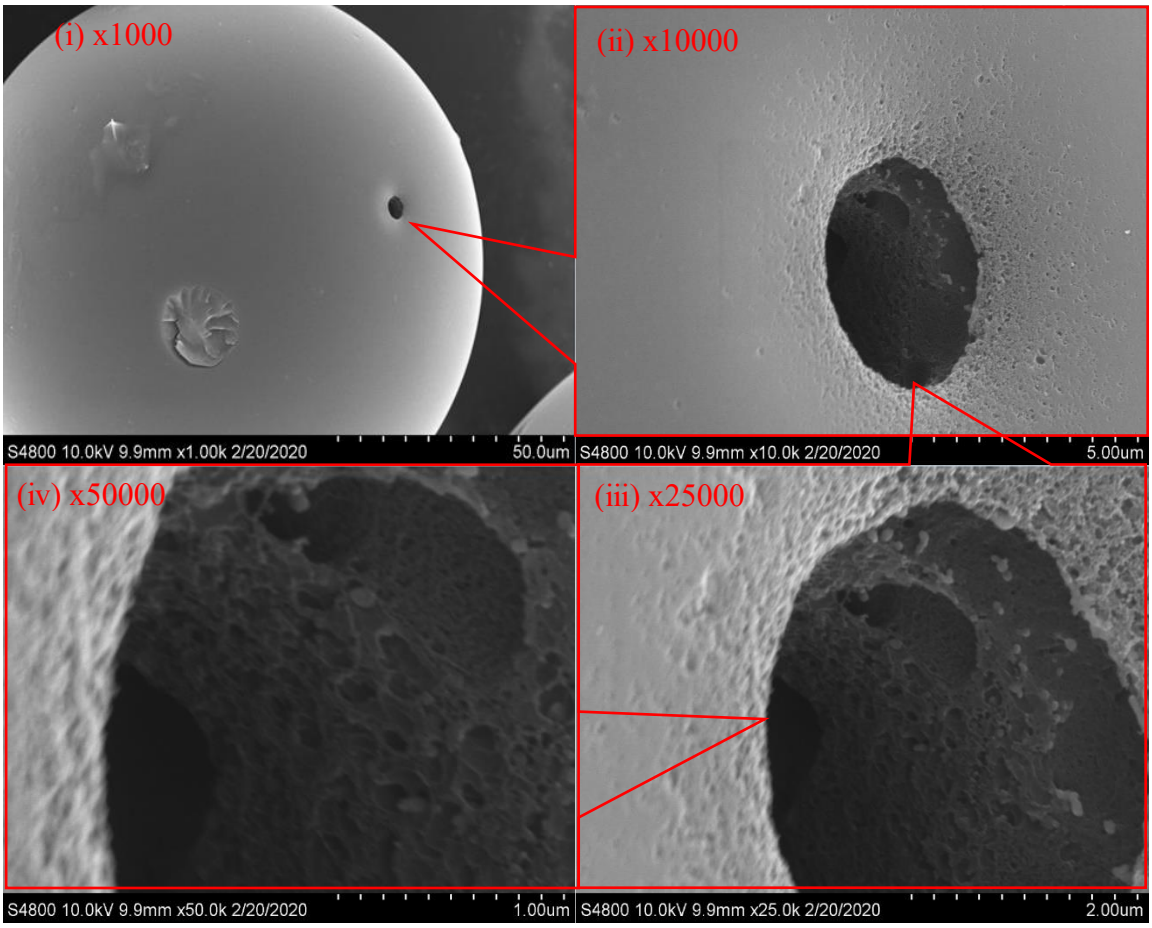

Figure 4-2 The SEM image of ACS surface for (i) 1000x, (ii) 10000x, (iii) 25000x, and (iv) 50000x magnification

doi:10.6342/NTU202002980

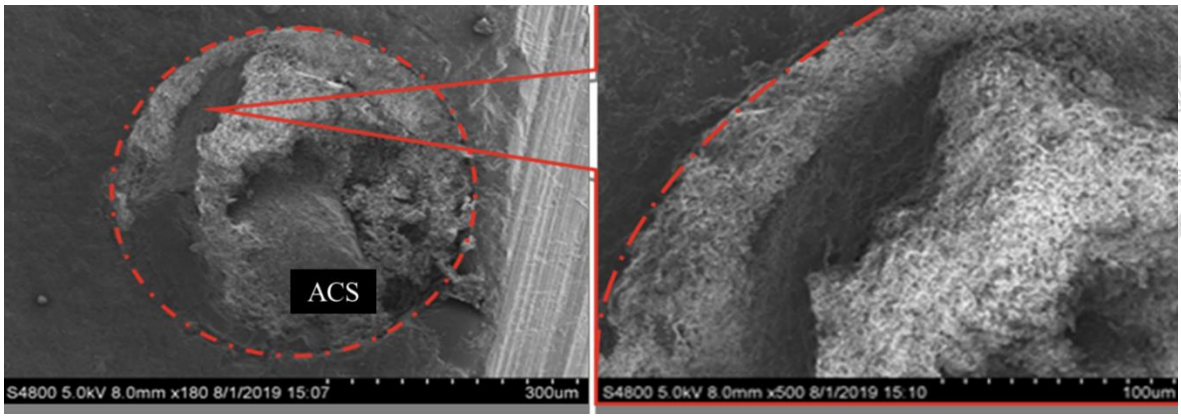

Figure 4-3 The SEM image for ground ACS

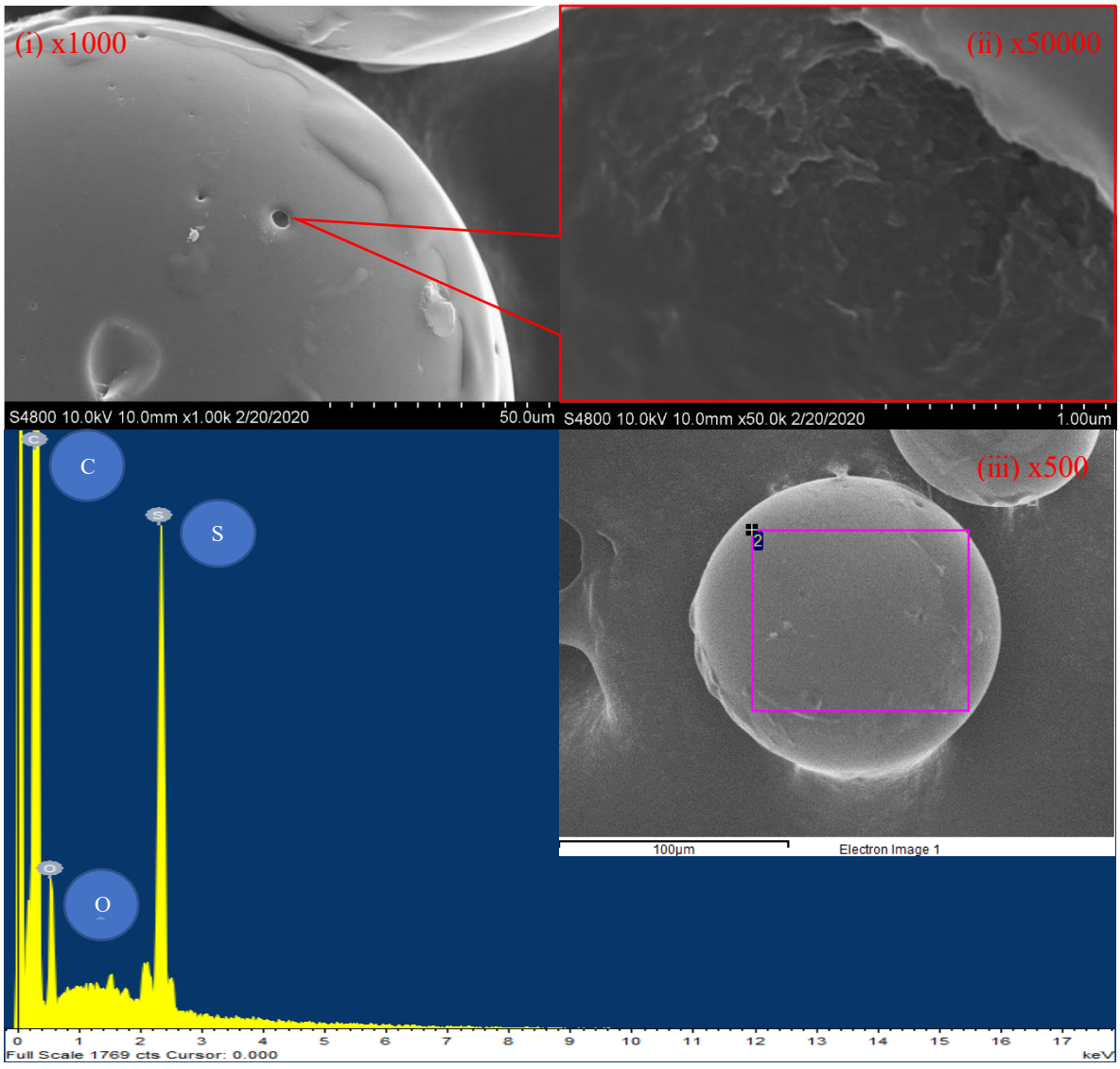

Figure 4-4 The SEM image of TUACS for (i) 1000x, and (ii) 50000x magnification; (iii) EDX image of TUACS

doi:10.6342/NTU202002980

Figure 4-5 The photo of TUACS-Au

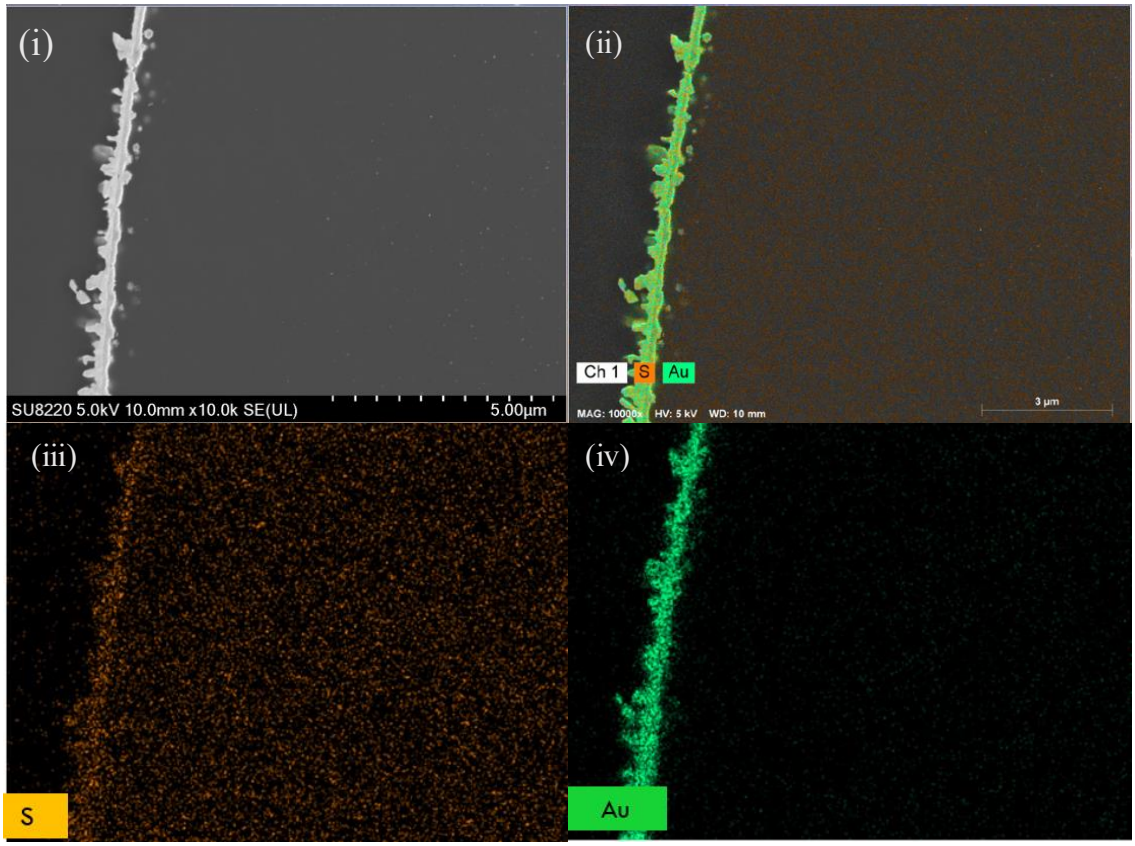

Figure 4-6 The SEM image of (i) the ground TUACS-Au and the mapping image of (ii) S and Au elements, (iii) S element, and (iv) Au element inside the TUACS-Au

doi:10.6342/NTU202002980

4.1.3 Transmission Electron Microscopy (TEM)

To visualize the crystal composition of ACS and TUACS, the TEM images are shown in Figure 4-8 and Figure 4-7. In Figure 4-8, three–dimensional micropores are randomly distributed inside the ACS. In Figure 4-7, after TU modification, the surface structure of TUACS became flaky, resembling the structure of graphene oxide. This proves that the thiourea changed the surface structure of ACS.

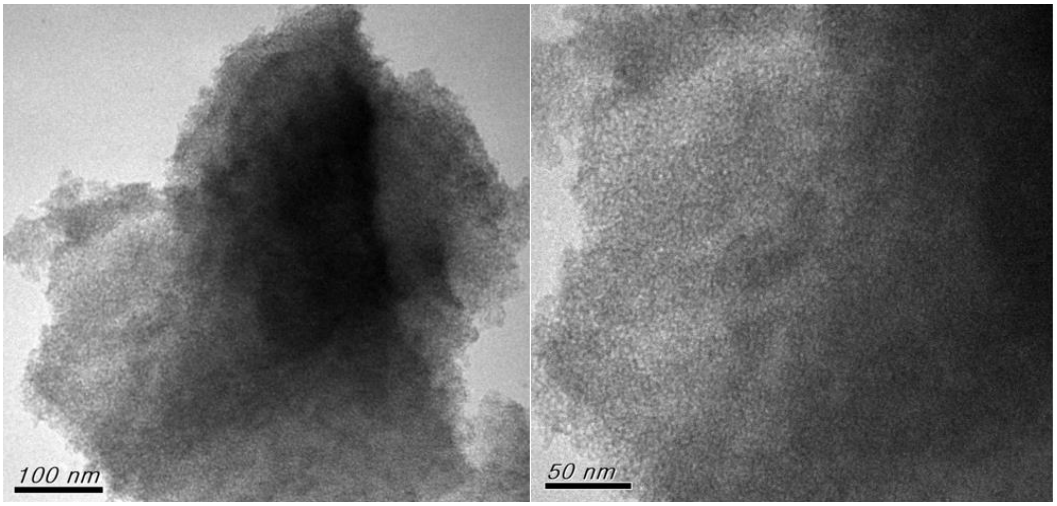

Figure 4-8 TEM image of ACS

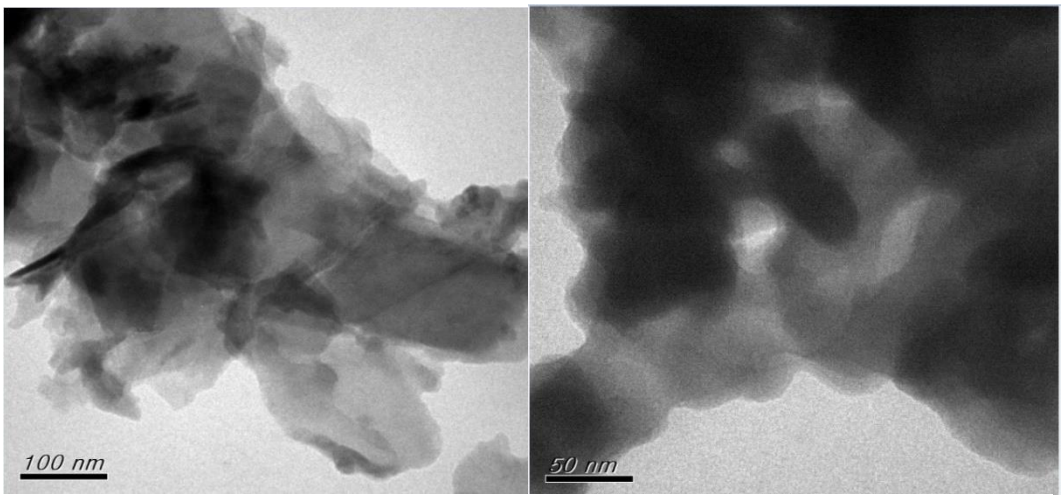

Figure 4-7 TEM image of TUACS

doi:10.6342/NTU202002980

4.1.4 Specific surface area, pore volume, and pore size distribution (PSD)

The specific surface area and pore volume were analyzed using the BET and t-plot methods, as shown in Table 4-2. The BET surface area and micropore volume of TUACS decreased in comparison with ACS's, which means that thiourea may be adsorbed not only on the surface but also in the micropore region of ACS. The mesopore size distribution was analyzed based on the BJH method with Halsey thickness curves, and micropore size distribution was analyzed with N_2 at 77K based on the NLDFT method assuming carbon slit pores geometry, shown in Figure 4-9, which clearly illustrated that both ACS and TUACS were micropore-intensive materials, but a decrease in both micropore size and amount was observed after TU modification.

doi:10.6342/NTU202002980

Table 4-2 The pore and surface properties of ACS and TUACS

Properties	**ACS**	**TUACS**
BET surface area ($m^2 g^{-1}$)	2445	1902
Micropore area ($m^2 g^{-1}$)	1990	973.9
External surface area ($m^2 g^{-1}$)	455.6	928.1
Total pore volume ($m^3 g^{-1}$)	1.081	0.913
Micropore volume ($m^3 g^{-1}$)	0.812	0.418
Average pore diameter (nm)	1.768	1.921

doi:10.6342/NTU202002980

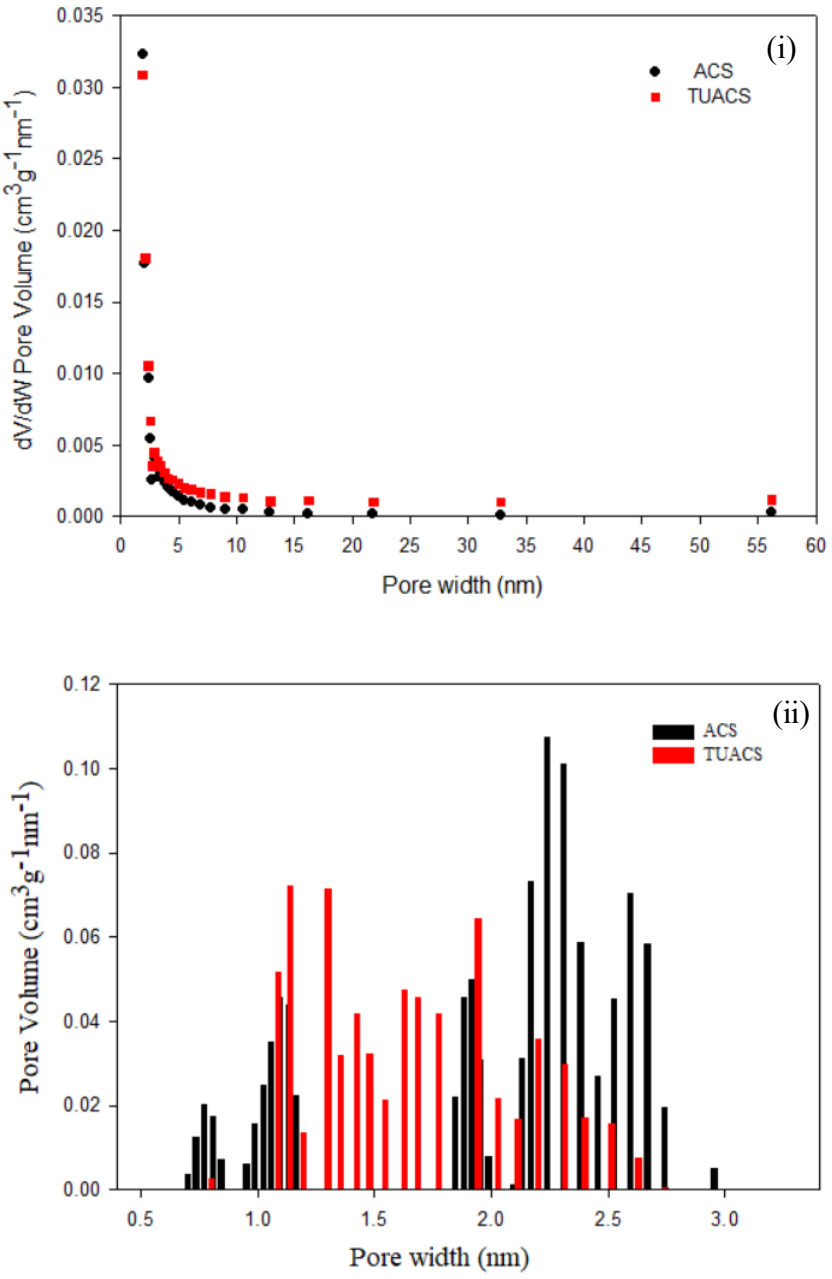

Figure 4-9 (i) Mesopore size distribution of ACS and TUACS

(ii) Micropores size distribution of ACS and TUACS

doi:10.6342/NTU202002980

4.1.5 Raman spectroscopy

Raman spectra of ACS and TUACS are shown in Figure 4-10. The D band represents the degree of defect and disorder, and the G band represents the degree of graphitization. ACS had a peak in the D band located at around 1298 cm^{-1} and a peak in the G band located at around 1591 cm^{-1}. In addition, TUACS had peaks in the D and G bands located at around 1292 cm^{-1} and 1603 cm^{-1}, respectively. The G/D intensity ratio (I_g/I_d) indicates the graphitic structure regarding the degree of structural disorder and defects (Fan, et al., 2014). The I_g/I_d values of both ACS and TUACS were 0.9, which meant a high degree of graphitization.

Additionally, I_V is the intensity of a valley between the G and D band peak. The I_V/I_G ratio has been used as an indication to measure the degree of disorder and the proportion of amorphous carbon (Dong, et al., 2009; Rajagopal, et al., 2016). In this study, I_V/I_G of ACS was 0.81, and that of TUACS was 0.79, where higher I_V/I_G ratios imply a higher proportion of amorphous materials. This also implies the presence of sp^2 carbons and amorphous content in both materials.

doi:10.6342/NTU202002980

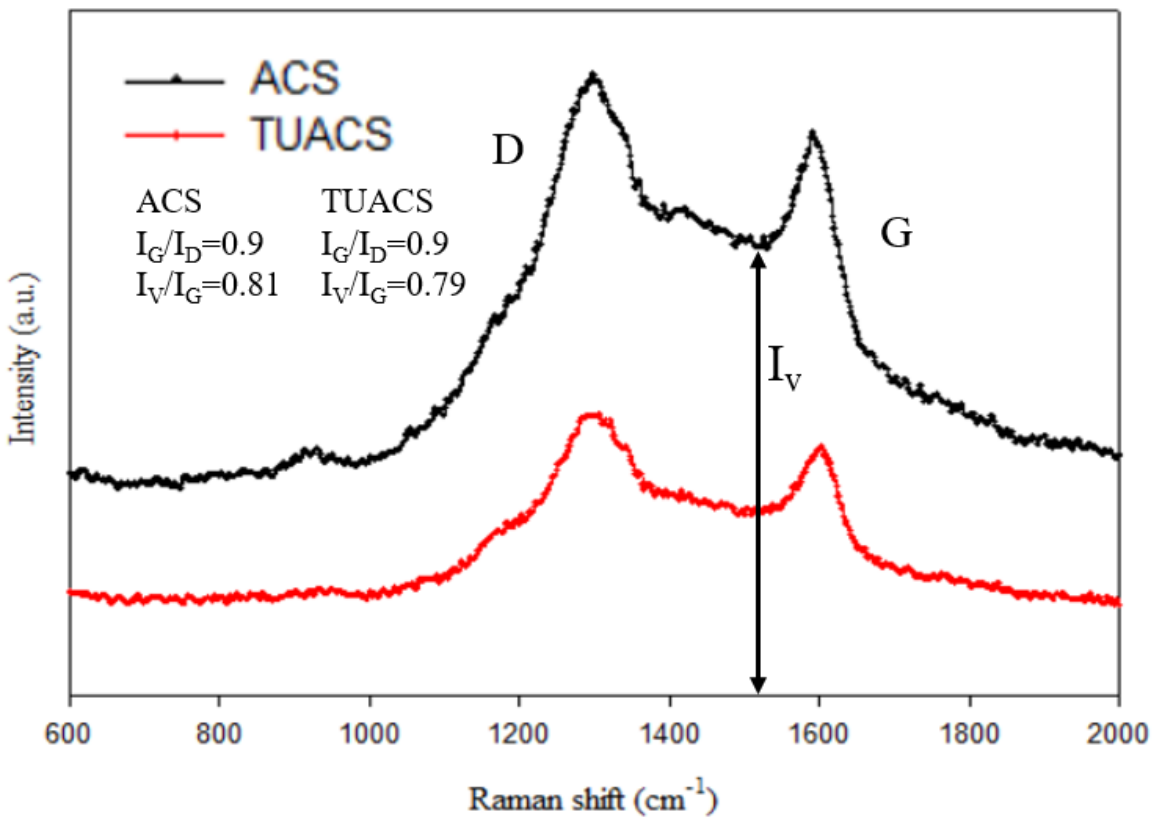

Figure 4-10 Raman spectra of ACS and TUACS

doi:10.6342/NTU202002980

4.1.6 X-ray Diffraction (XRD)

Figure 4-11 depicts the XRD patterns of ACS and TUACS. The pattern was recorded in the scan range 2θ= 10°-90°, at a scan rate of 4 s/step. There was only a weak peak of graphite centered at 44°, corresponding to (101) plane in the ACS and TUACS patterns. Since a high temperature of 900°C was used to activate the ACS, the pattern resulted in a turbostratic and amorphous structure (Fan et al., 2014; McDougall & Hancock, 1981).

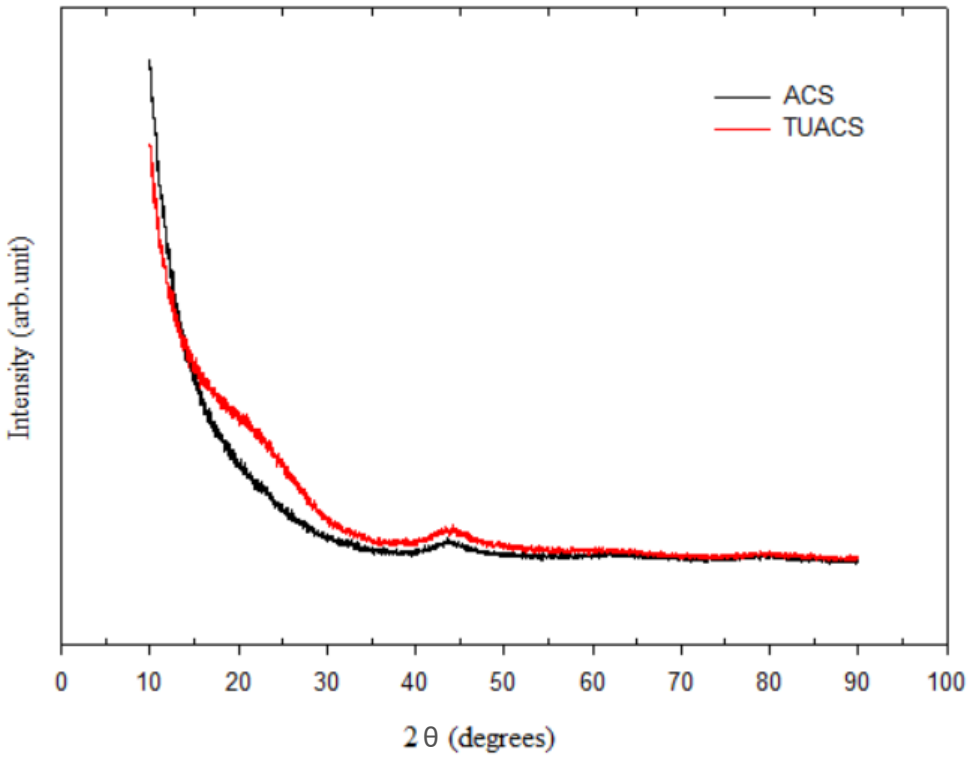

Figure 4-11 X-ray diffraction patterns of ACS and TUACS

doi:10.6342/NTU202002980

4.1.7 X-ray Photoelectron spectroscopy (XPS)

The XPS analysis was conducted for understanding the functional groups on the surface of the ACS and TUACS, as shown from Figure 4-12 to Figure 4-14.

In Figure 4-12(i), the results of the binding energy of the C1s of ACS are displayed. It can be seen that there were two main peaks located at the binding energies of 286.6 and 284.7 eV, which represent the binding energies of ether (C-O-C) and graphitic carbon (C-C), respectively. In Figure 4-12(ii), the results of the binding energy of the O1s of ACS are demonstrated. The main peak at 533.0 eV corresponds to C-O-C, and the peak at 530.4 eV corresponds to C-OH. (Burg et al., 2002; Li et al., 2019; Terzyk, 2001)

In Figure 4-13(i), the results of the binding energy of the C1s of TUACS are illustrated. The main peak at 284.8 eV corresponds to C-C, the peak at 286.2 eV corresponds to C-O-C, and the peak at 286.8 eV corresponds to C-OH. In Figure 4-13(ii), the results of the binding energy of O1s of TUACS are illustrated. The main peak at 532.8 eV corresponds to C-O-C (Burg et al., 2002; Li et al., 2019; Terzyk, 2001). Compared with Figure 4-12(ii) and Figure 4-13(ii), the C-O-C bond increased slightly in Figure 4-13(ii), and the percentage of C-OH bonds decreased from 5.9% to 0 in Figure 4-13(ii).

In Figure 4-15, the results of the binding energy of S2p of TUACS are illustrated. The main peak at 163.9 eV corresponds to C-S ($2p_{3/2}$), the peak at 165.1 eV corresponds to C-S

doi:10.6342/NTU202002980

($2p_{1/2}$) (Kwak et al., 2017). The peak at 168.8 eV corresponds to the sulfite ion (SO_3^{2-}) (Li et al., 2014).

Figure 4-14 illustrates the results of the binding energy of Au4f of TUACS-Au. There are two main peaks at 83.7 eV and 87.4 eV corresponding to Au^0, indicating that $AuCl^-$ was successfully reduced to Au element on the surface of TUACS (Chou & McFarland, 2004).

doi:10.6342/NTU202002980

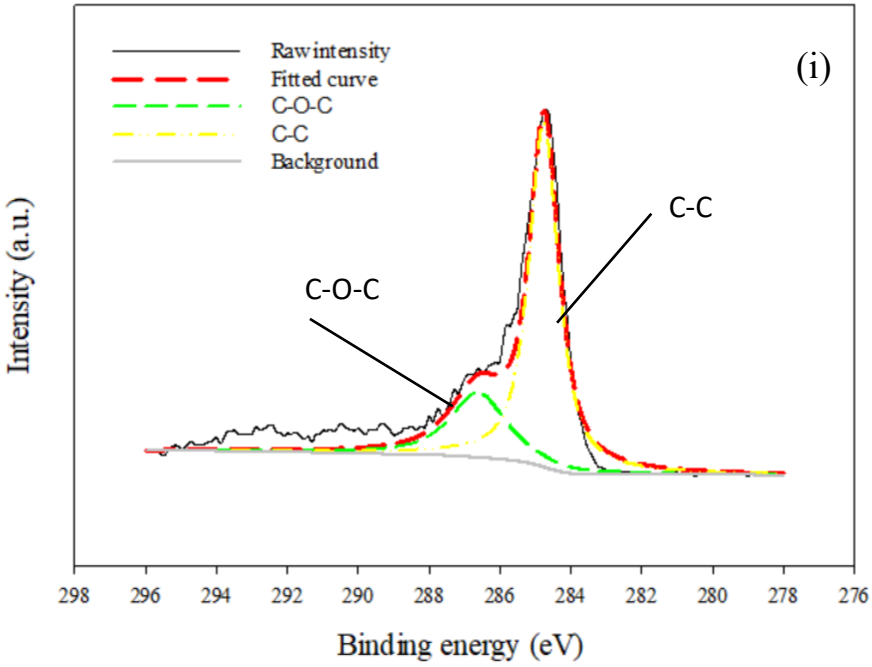

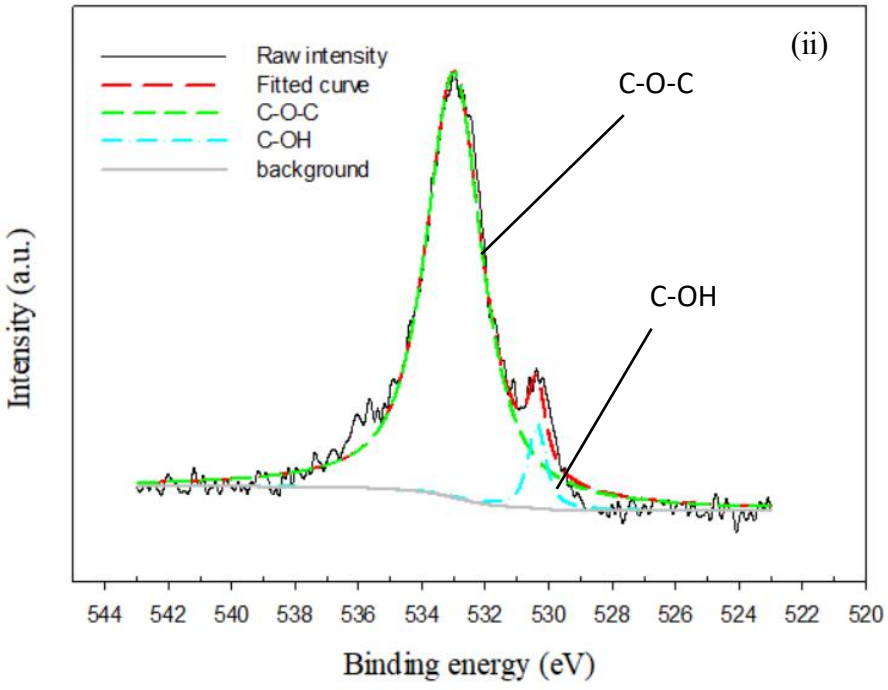

Figure 4-12 ACS's XPS spectra of (i) C1s and (ii) O1s

doi:10.6342/NTU202002980

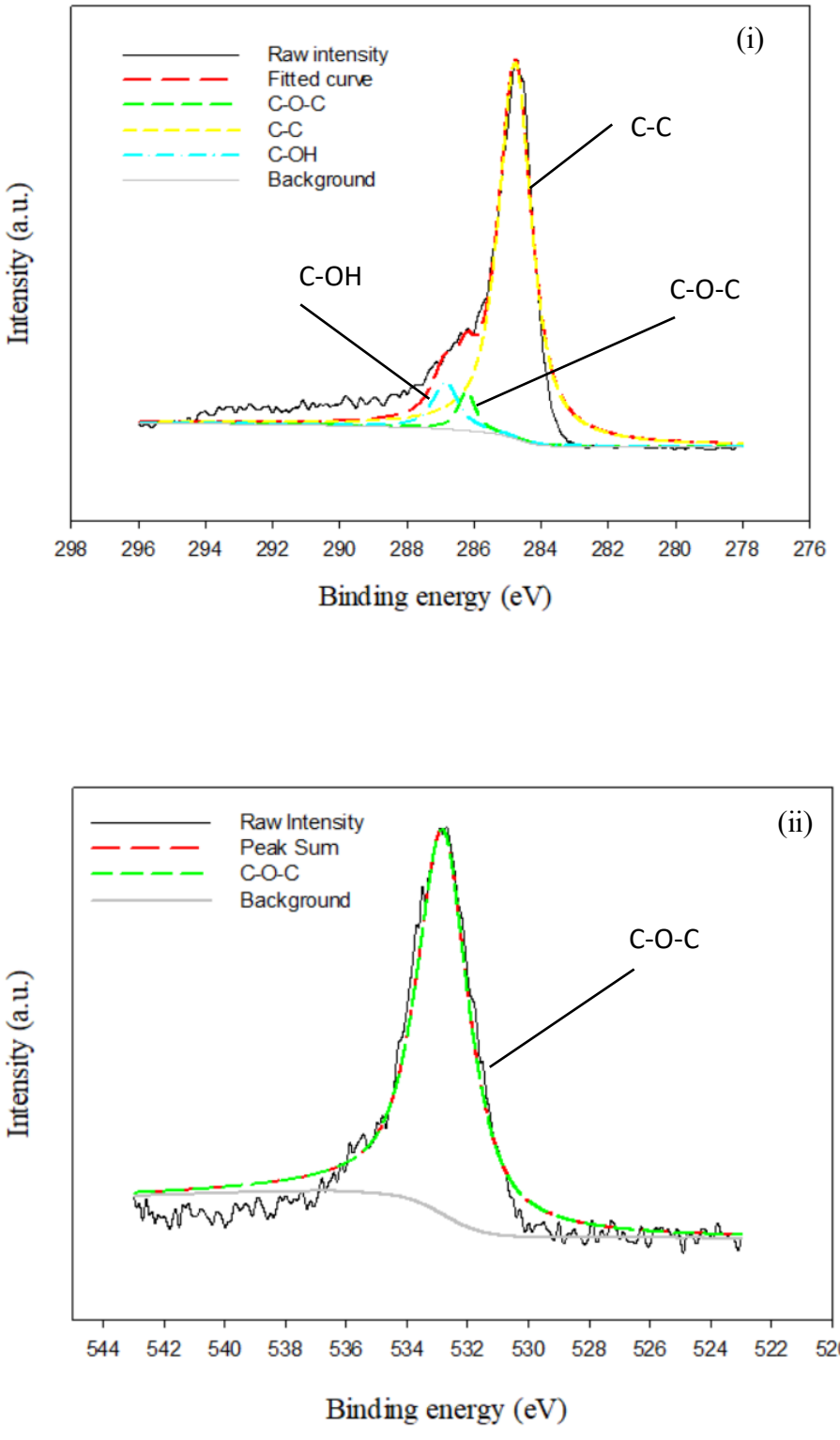

Figure 4-13 TUACS's XPS spectra of (i) C1s and (ii) O1s

doi:10.6342/NTU202002980

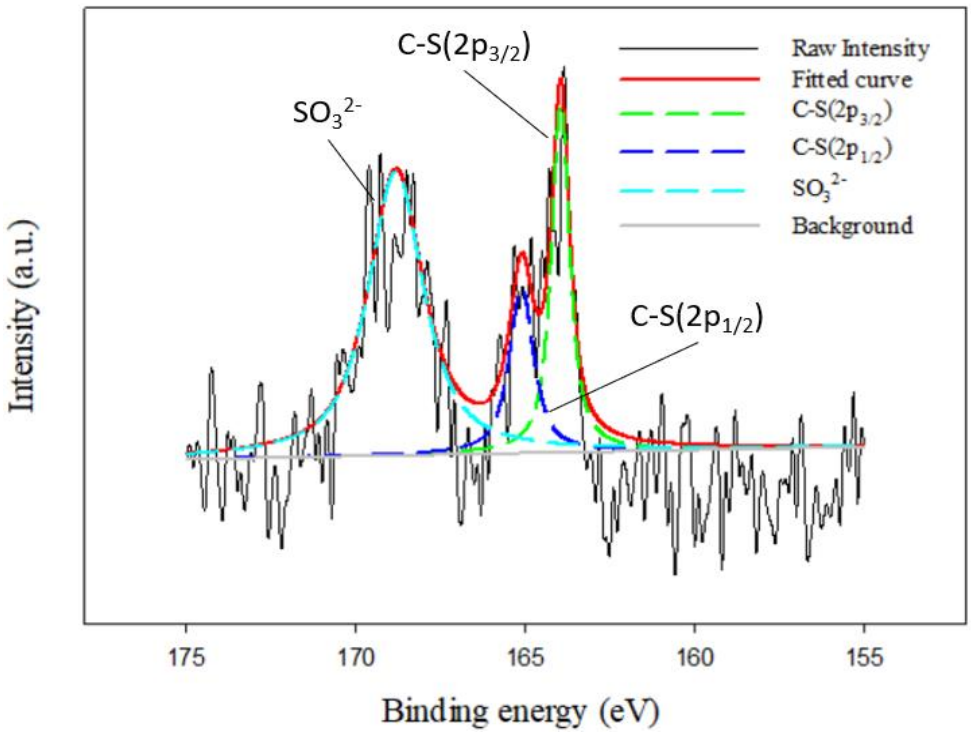

Figure 4-15 TUACS's XPS spectra of S2p

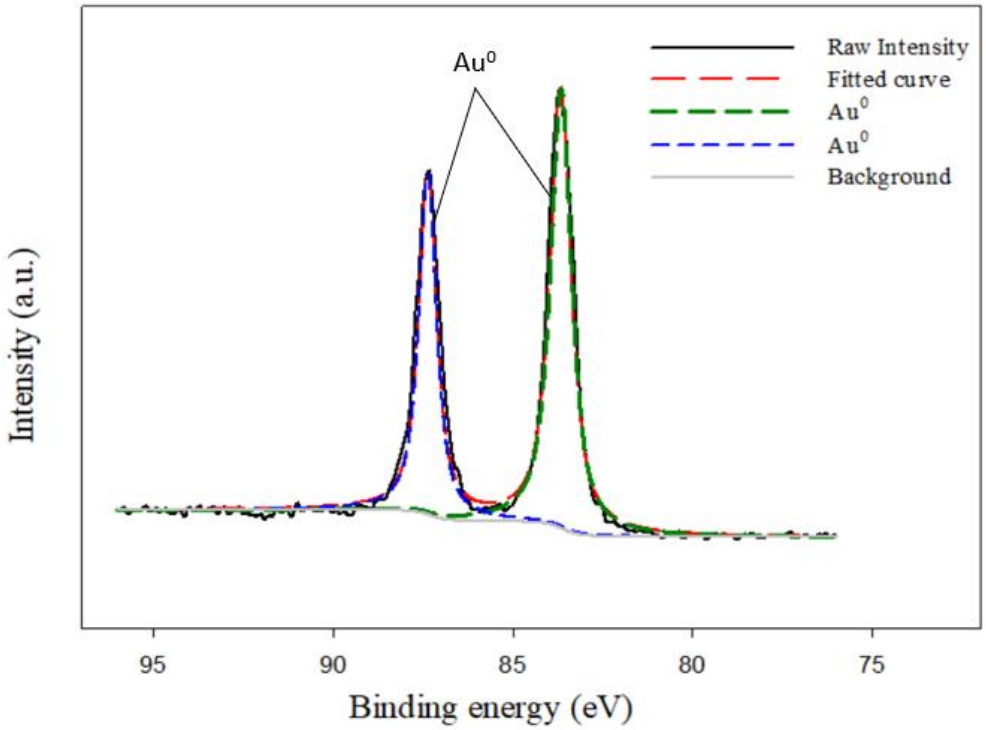

Figure 4-14 TUACS-Au's XPS spectra of Au4f

doi:10.6342/NTU202002980

4.2 Adsorption experiments of Au by TUACS

4.2.1 Effect of contact time

For determining the adsorption kinetics of TUACS for Au, the contact times of 12, 24, 48, 72, 96 and 120 h were selected. The initial concentration of the Au ion solution was 10 mg L^{-1}, the dosage of TUACS was 0.01 g L^{-1}, the temperature of the reciprocal shaking water bath was 30°C, the shaking velocity was 150 rpm, the pH value of the Au ion solution was 2, and the solution volume was 50 mL. The results of the experiment are shown in Figure 4-16. The time needed for saturated adsorption capacity was approximately 96 h. Moreover, the removal efficiency was 75±4.1%. Based on the removal efficiency, the Au capacity is calculated to be 750 mg g^{-1}. The reaction was considered to be controlled by chemisorption, as the reaction took a long time to reach equilibrium. It also proves that the sulfur on the TUACS forms a bond with the Au ions.

doi:10.6342/NTU202002980

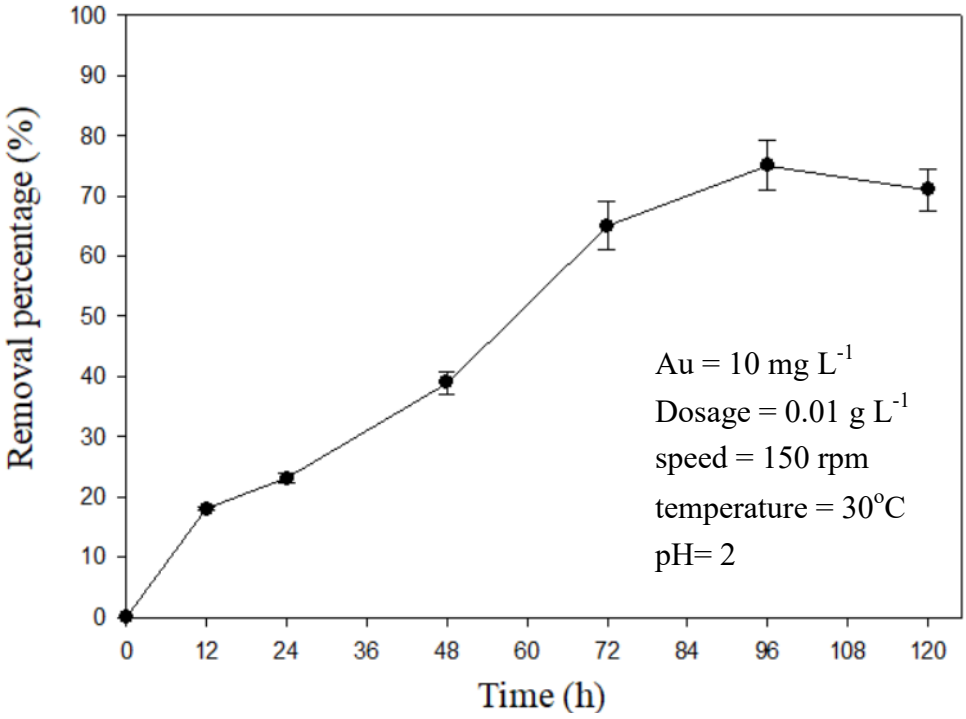

Figure 4-16 Effect of contact time on gold removal efficiency by TUACS

doi:10.6342/NTU202002980

4.2.2 Effect of pH value

pH value was considered as an essential parameter as it could affect the removal percentage. Figure 4-17 shows the removal percentage of Au at different initial pH levels from 0.5 to 10.0. As the pH increased from 0.5 to 2.0, the Au removal capacity also increased. Nevertheless, the Au capacity gradually decreased as the pH value increased from 2.0 to 10.0, indicating that the optimum pH was 2.0. Below pH=2.0, the dominant gold species, $AuCl_4^-$, and Cl^- competed for adsorption sites, resulting in a reduced gold ion removal percentage (Li et al., 2013). Above pH=6.0, the dominant Au species became $AuCl_3(OH)^-$, $AuCl_2(OH)_2^-$ and $AuCl(OH)_3^-$, $Au(OH)_4^-$, $Au(OH)_3$, resulting in an electrostatic repulsion between Au ions (García-Soto & González-Ortega, 2016; Lin et al., 2018). The speciation reactions for gold chloride are shown in Eqs. (4-1) to (4-6).

$$AuCl_4^- \rightleftharpoons Au^{3+} + 4Cl^- \qquad \log K = -25.2 \qquad (4\text{-}1)$$

$$AuCl_3(OH)^- \rightleftharpoons Au^{3+} + 3Cl^- + OH^- \qquad \log K = -33.34 \qquad (4\text{-}2)$$

$$AuCl_2(OH)_2^- \rightleftharpoons Au^{3+} + 2Cl^- + 2OH^- \qquad \log K = -40.3 \qquad (4\text{-}3)$$

$$AuCl_4^- \rightleftharpoons Au^{3+} + Cl^- + 3OH^- \qquad \log K = -45.94 \qquad (4\text{-}4)$$

$$Au(OH)_4^- \rightleftharpoons Au^{3+} + 4OH^- \qquad \log K = -51.35 \qquad (4\text{-}5)$$

$$Au(OH)_3 \rightleftharpoons Au^{3+} + 3OH^- \qquad \log K = -44.95 \qquad (4\text{-}6)$$

doi:10.6342/NTU202002980

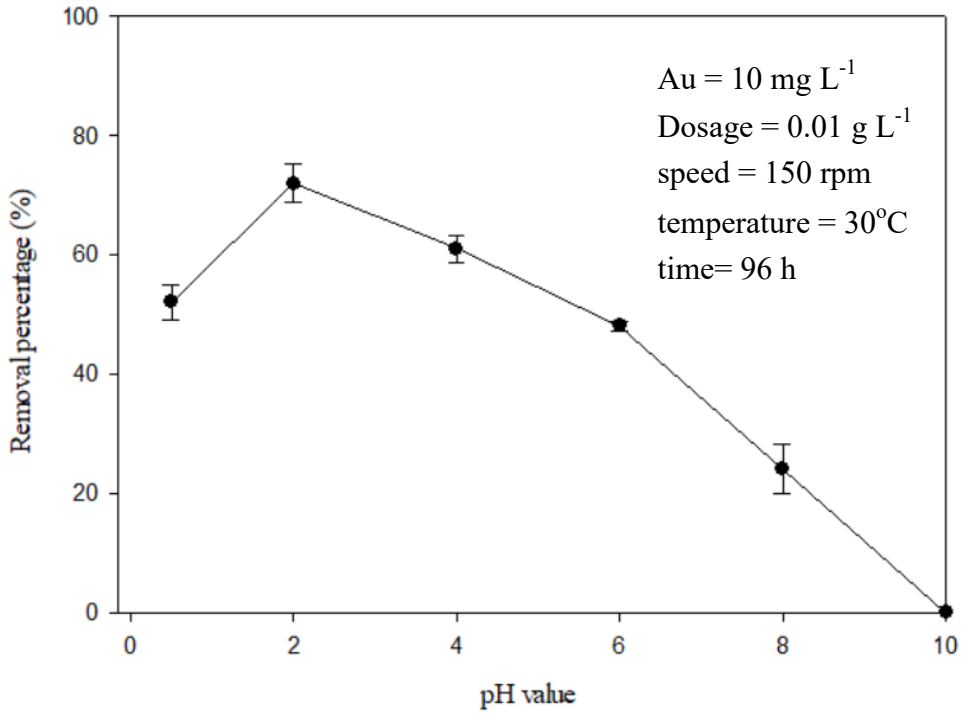

Figure 4-17 Effect of pH on the removal percentage of gold.

doi:10.6342/NTU202002980

4.2.3 Effect of TUACS dosage

TUACS dosages of 0.01, 0.02, 0.03, 0.04, 0.05, 0.06, 0.07 g L^{-1} were selected to determine the removal efficiency of gold in liquid phase. The initial concentration of gold ion solution was 10 mg L^{-1}, the temperature of the reciprocal shaking water bath was 30°C, the shaking velocity was 150 rpm, the pH value of the gold ion solution was 2, and the solution volume was 50 mL. It could be clearly seen from Figure 4-18 that the removal percentage rose gradually from 72% at 0.01 g L^{-1} to 99% at 0.06 g L^{-1}. Hence, the dosage of 0.06 g L^{-1} was chosen for subsequent experiments because it had the best removal performance.

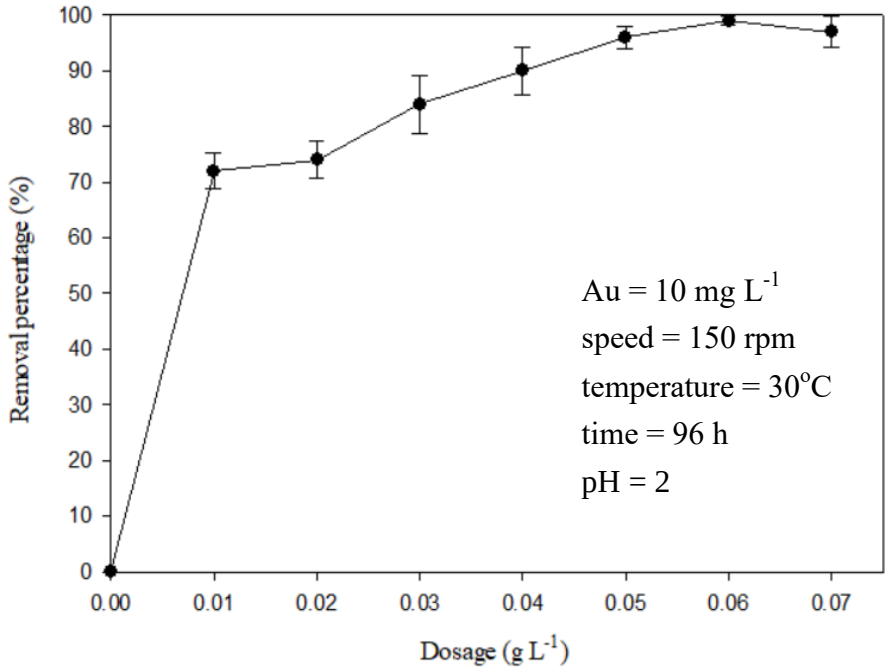

Figure 4-18 Effect of TUACS dosage on the removal percentage of gold.

doi:10.6342/NTU202002980

4.2.4 Adsorption isotherm experiments of TUACS

Based on the Langmuir, Freundlich, and Temkin isotherms, the adsorption mechanism of the adsorbent could be determined. The initial concentration of the Au ion solution (C_0) was 10, 20, 30, 40, 50 mg L^{-1}; the temperature of the reciprocal shaking water bath was 30°C, the shaking velocity was 150 rpm, the pH value of gold ion solution was 2, and the solution volume was 50 mL. Figure 4-19, Figure 4-20, and Figure 4-21 illustrates three isotherm results. In Figure 4-19, the Langmuir fitted model was obtained by plotting C_e versus q_e/C_e. the squared correlation parameter (R^2) was 0.91, the Langmuir adsorption constant (K_L) was 0.0962 L mg^{-1}, and the theoretical maximum adsorption capacity (Q_m) was 2000 mg g^{-1}. The separation factor S_F was between 0 and 1 and indicated a favorable sorption.

In Figure 4-20, the Freundlich isotherm constants K_F and n were 321.81 L mg^{-1} and 2.151, respectively; however, the squared correlation parameters (R^2) was 0.75. The value of R^2 for Freundlich isotherm was lower than those for Langmuir and Temkin isotherms; therefore, the adsorption behavior does not follow Freundlich isotherm closely.

In Figure 4-21, the Temkin isotherm constants a and b were 0.928 and 5.486, respectively. The squared correlation parameters (R^2) was 0.8. The value of R^2 was lower than Langmuir, therefore, the adsorption behavior was more appropriate for Langmuir isotherm. Thus, it suggests that the adsorption process is mainly controlled by monolayer coverage.

doi:10.6342/NTU202002980

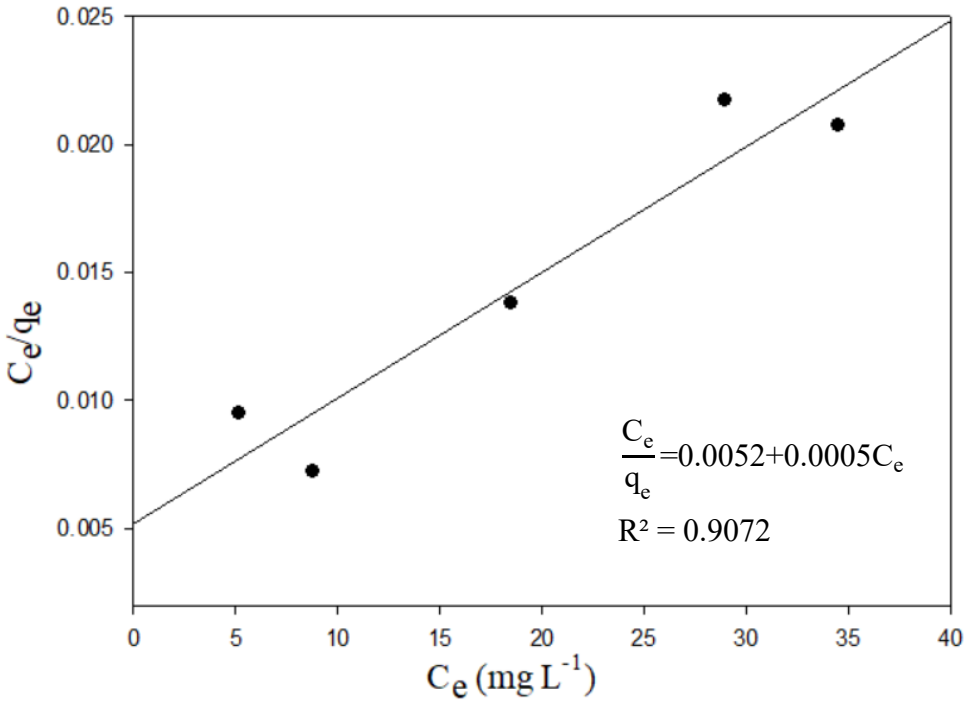

Figure 4-19 Results of Langmuir isotherm model of TUACS

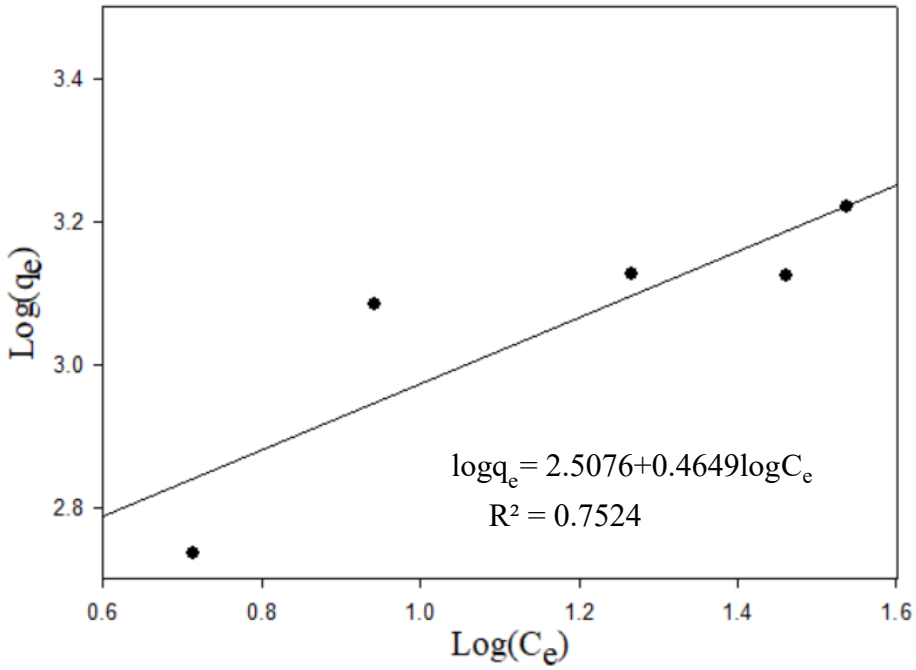

Figure 4-20 Results of Freundlich isotherm model of TUACS

doi:10.6342/NTU202002980

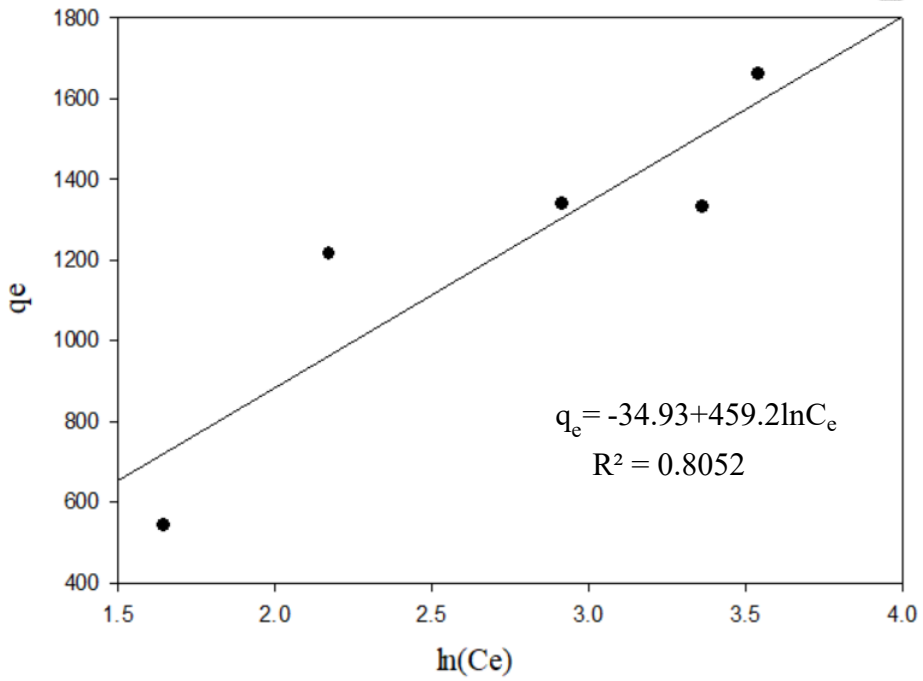

Figure 4-21 Results of Temkin isotherm model of TUACS

doi:10.6342/NTU202002980

4.3 Comparison of selective adsorption capacity by carbonized PF resin spheres and TUACS

To compare the selective adsorption efficiencies of carbonized PF resin spheres and TUACS, selective adsorption experiments were conducted. The conditions of the experimental variables were as follows: The initial concentration of the gold ion solution was 10 mg L^{-1}, the temperature of reciprocal shaking water bath was 30°C, the shaking velocity was 150 rpm, the pH value of the gold ion solution was 2, and the dosage was 0.06 g L^{-1}. In Figure 4-22, the PF resin sphere only carbonized and was imperfect for gold adsorption. However, after activation and modification with thiourea, the BET surface area increased and $\pi - \pi$ interaction between aromatic organic carbon spheres promoted the adsorption. Moreover, the thiourea modified activated carbon sphere had better adsorption efficiency, since a gold–sulfur bond was formed (Chen et al., 2020). Moreover, TUACS had a selective adsorption characteristic because the oxygen functional groups were in low proportions.

doi:10.6342/NTU202002980

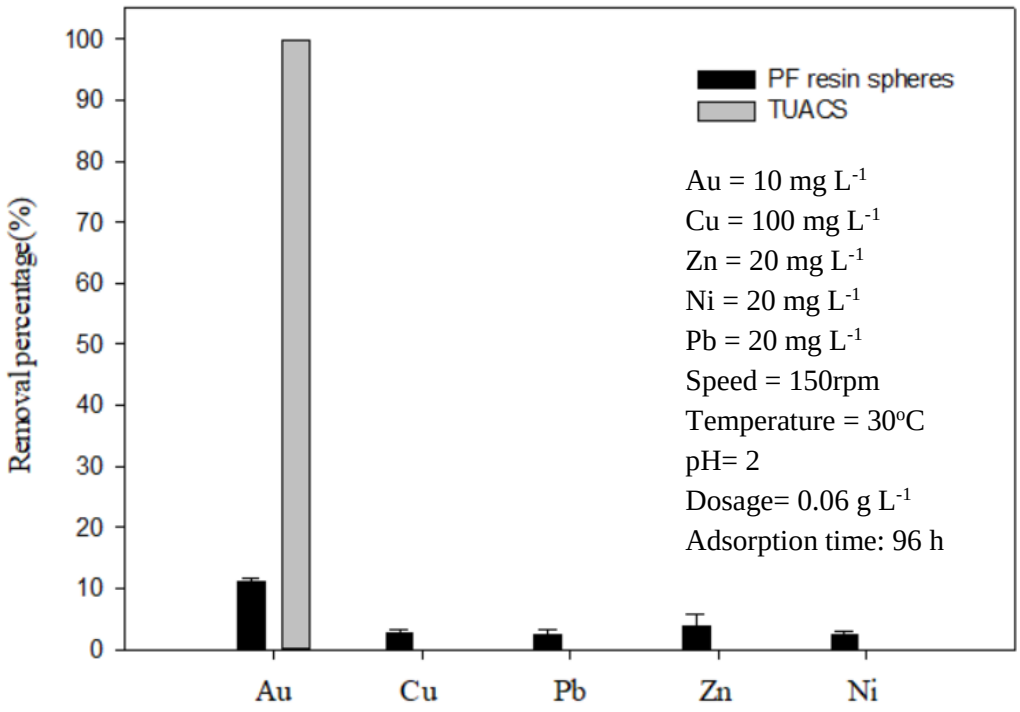

Figure 4-22 Selective adsorption results of high concentration of Au by carbonized PF resin sphere and TUACS

doi:10.6342/NTU202002980

4.4 Selective adsorption experiments by TUACS for real wastewater metal content

In order to simulate metal concentrations contained in wastewater of PCBs, the simulated wastewater was prepared with Cu of 100 mg L^{-1}, Pb, Zn, and Ni of 20 mg L^{-1}, and Au of 0.01 mg L^{-1}. These metal concentration percentages were based on Zhang et al. (2012), and the Au concentration was 1000 times lower than those present in previous experiments. Furthermore, the Cu concentration was 5 times higher than those in previous experiments. In these experiments, the temperature of the reciprocal shaking water bath was 30°C, the shaking velocity was 150 rpm, the pH value of gold ion solution was 2, and the dosage was 3mg/50 mL. As shown in Figure 4-23, TUACS showed excellent selective adsorption for Au. The removal efficiency of gold was 92%, without adsorption of other metals. The results proved that even in an extreme low concentration of Au, there was exceptional selective adsorption of Au by TUACS.

doi:10.6342/NTU202002980

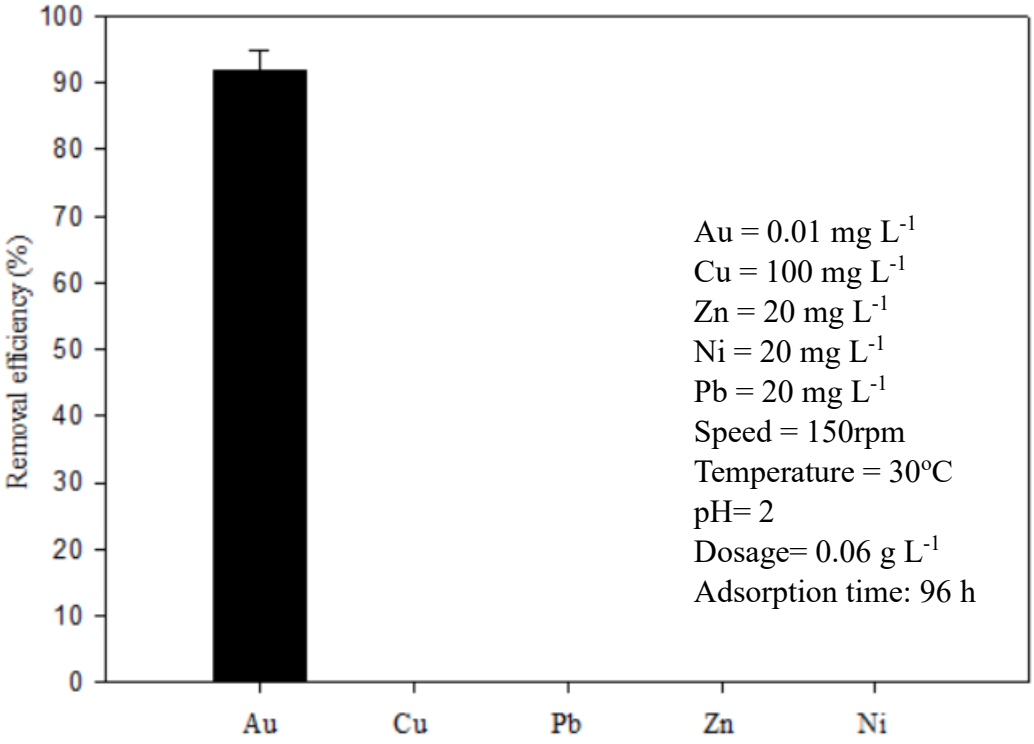

Figure 4-23 Selective adsorption results of low concentration of Au by TUACS

doi:10.6342/NTU202002980

4.5 Desorption experiments of Au

To strip Au from TUACS, we used ammonium thiosulfate $(NH_4)_2S_2O_3$ as a leaching agent. The concentrations of $(NH_4)_2S_2O_3$ were 0.1, 0.2, 0.3, 0.4 M. Assuming that the removal efficiency of Au is 100%, the capacity of Au on 3 mg TUACS was 0.5 mg Au/3 mg TUACS (i.e., 166.7 g kg^{-1}), at the temperature of reciprocal shaking water bath of 30°C, the shaking velocity of 150 rpm, and the desorption time of 24 h. The desorption efficiencies were 83%, 73%, 94%, and 88%, for concentrations of 0.1, 0.2, 0.3, and 0.4 M, respectively (Figure 4-24). According to the results, 0.3 M had better desorption efficiency, so this concentration was chosen for the following regeneration experiments.

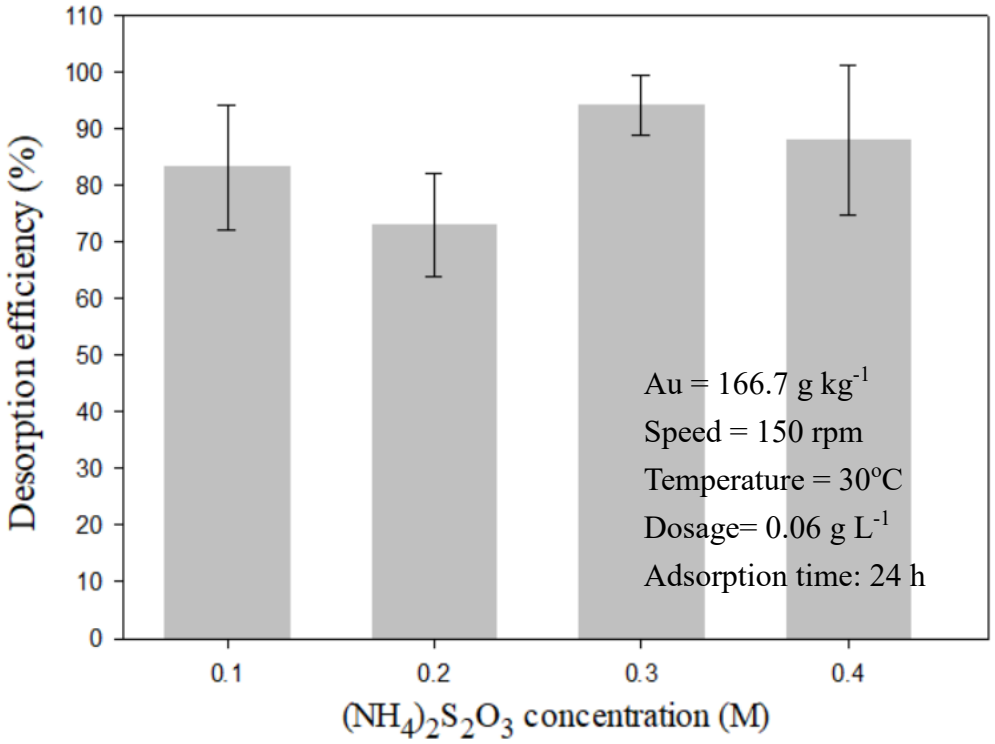

Figure 4-24 Effect of ammonium thiosulfate concentration for Au desorption

doi:10.6342/NTU202002980

4.6 Repeated adsorption and desorption experiments of Au

To understand the reusability of TUACS, repeated adsorption and desorption experiments of Au were conducted. For adsorption experiments, the initial concentration of Au was 10 mg L^{-1}. 3 mg of TUACS were added into 50 mL Au solution. The solution with TUACS was shaken in a reciprocal shaking water bath for 96 h at pH 2, 150 rpm, and 30^{o}C. For desorption experiments, the post-adsorption TUACS sample was added to 50 mL of 0.3 M ammonium thiosulfate for 24 h, and the adsorption and desorption experiments were repeated five times. The results are illustrated in Figure 4-25, which shows that after five cycles of adsorption and desorption experiments, the removal efficiency of gold was still > 90%. Hence, TUACS is an excellent material for reuse in Au recovery by adsorption.

doi:10.6342/NTU202002980

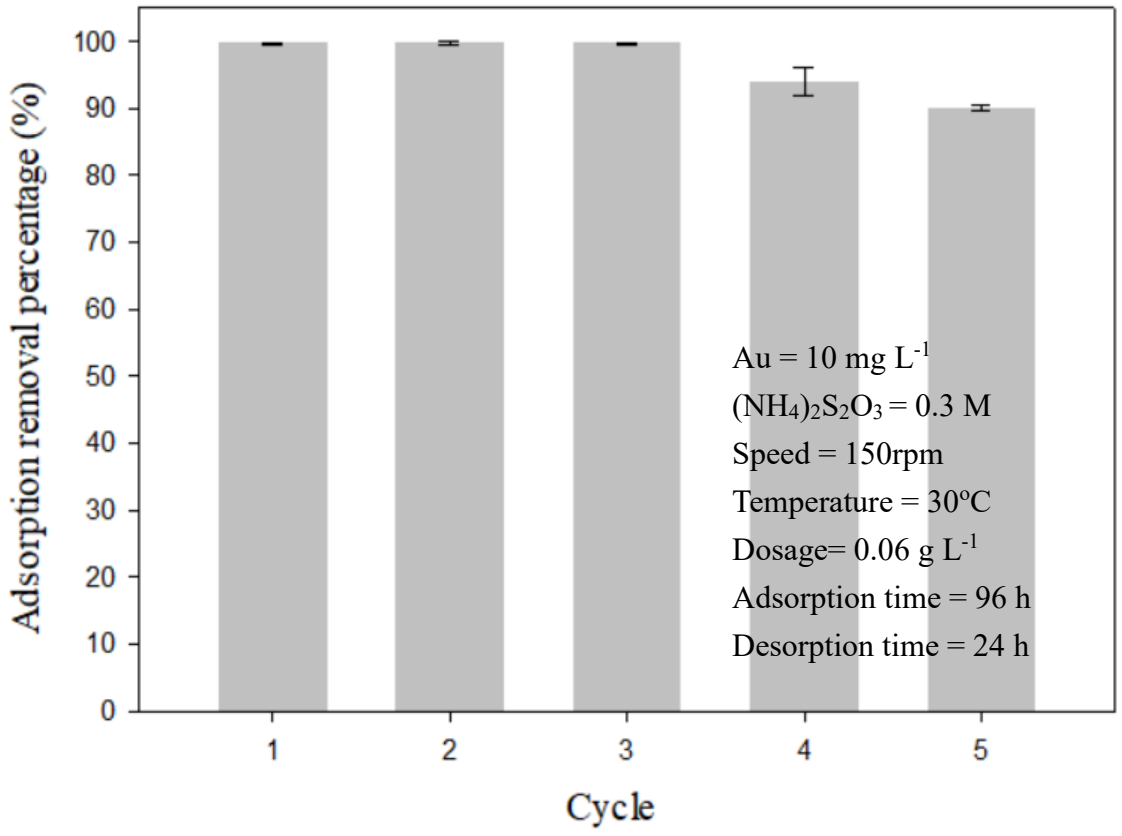

Figure 4-25 Repeated adsorption and desorption experiments for five times

doi:10.6342/NTU202002980

4.7 Mechanism

The mechanisms of TUACS synthesis and Au adsorption and desorption are shown in Figure 4-26, which contains three steps. (1) After the modification of thiourea, the thiophene bond and sulfur oxides exist in the TUACS according to XPS results in Figure 4-14. (2) Based on previous studies (Chen et al., 2020; X. Li et al., 2014), the adsorption ability of activated carbon depends on the large surface area and the π electrons on activated carbon's graphene crystallite. The TUACS has a large BET surface area of about 1900 $m^2 g^{-1}$ as shown in Table 4-2, so the Au could be reduced on the surface of the TUACS. Another pathway for Au adsorption is that sulfur atoms could bond with Au. Thus, it would increase the Au capacity. (3) The Au on the surface of TUACS can be desorbed by ammonium thiosulfate to form $Au(S_2O_3)_2^{3-}$ complex. Since the stability constant of $Au(S_2O_3)_2^{3-}$ (logβ) is 26, it would be a stable complex in solution (Štofková & Štofko, 2002).

According to the hard and soft acids and bases (HSAB) principle, the hardness value of Au^{3+} is smaller than Cu^{2+} and Pb^{2+}, meaning that Au^{3+} has greater tendency to bond to soft bases (aromatic sheets) on the TUACS. Besides, Au^{3+} had high redox potential E^0 ($AuCl_4^-$ /Au=1.0 V), so it can be simply reduced on the surface of TUACS. Moreover, the pH is low (pH= 2) in this study and goes against the cationic exchange (Cu^{2+}, Pb^{2+}, Zn^{2+}, Ni^{2+}) with the weak acid surface groups of TUACS (Alfarra, Frackowiak, & Béguin, 2004). This could

doi:10.6342/NTU202002980

be the reason that TUACS has excellent selective adsorption characteristics to Au even with strong competitive metals present in great levels.

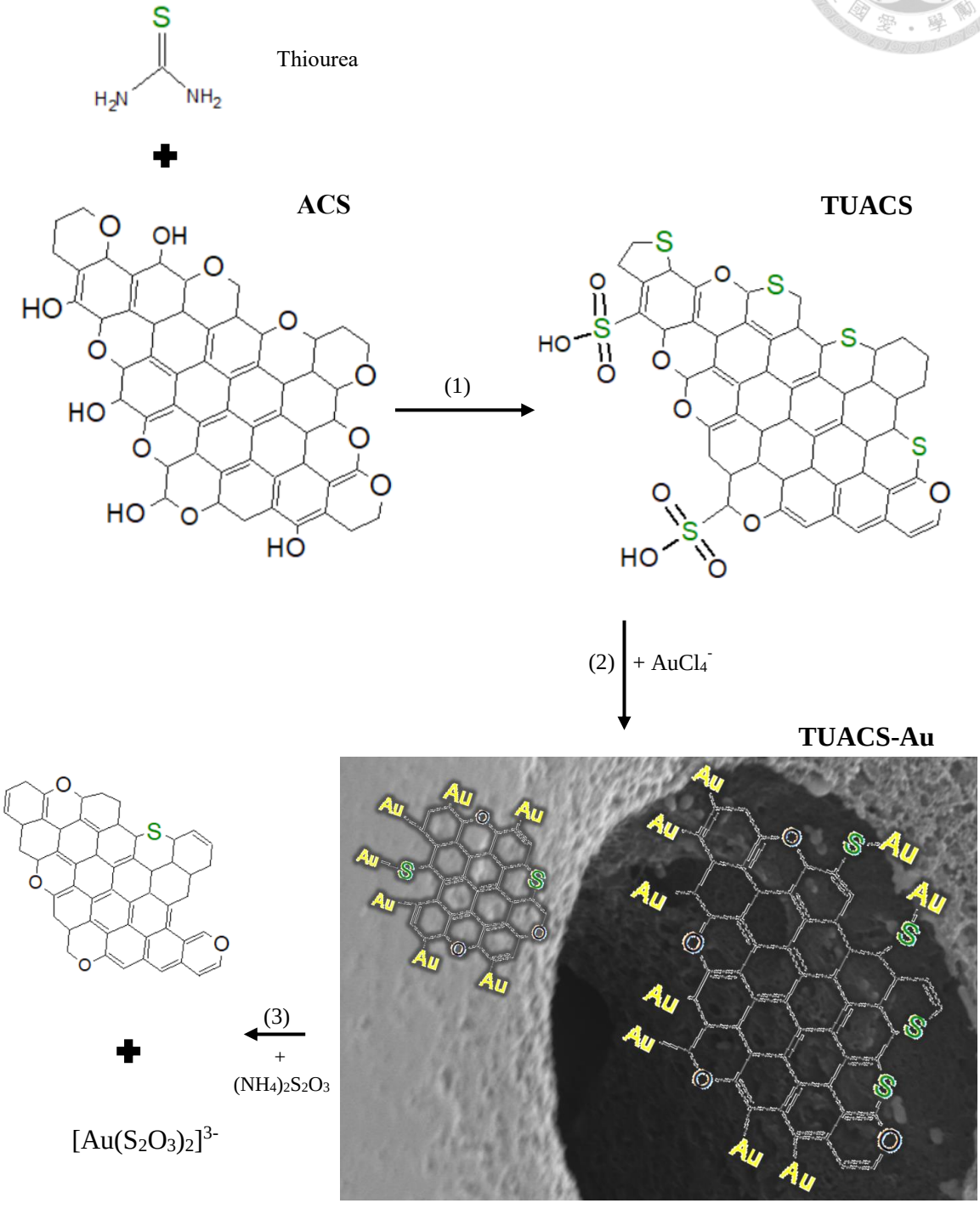

Figure 4-26 Mechanism of TUACS synthesized and gold adsorption and desorption

doi:10.6342/NTU202002980

Chapter 5 Conclusions and Suggestions

5.1 Conclusions

The purpose of this study is to develop a novel material to selectively recover gold (Au) in wastewater. This material is thiourea modified activated carbon sphere (TUACS), which has three vital features as described below:

1. TUACS has a high adsorption capacity and excellent selectivity for adsorption of gold. The test dosage of TUACS was 0.06 g L^{-1}; the initial gold concentration was 0.01 mg L^{-1}; the Cu ion concentration was 100 mg L^{-1}; the Pb, Zn, and Ni ion metals were 20 mg L^{-1}; the saturated adsorption time was 96 h at 30°C and pH= 2.0. The recovery of Au was about 92%, and no adsorption of other metals. The adsorption capacity is 750 mg g^{-1} when the initial concentration of Au = 10 mg L^{-1}.

2. The ammonium thiosulfate could successfully leach the Au from TUACS; the ammonium thiosulfate concentration was 0.3 M. The capacity of Au on 3 mg TUACS was 166.7 g kg^{-1}. The contact time was 24 h at 30°C and pH is 5.7. The desorption efficiencies could reach 94%.

3. For repeated adsorption and desorption experiments of Au, after five times cycle of adsorption and desorption experiments, the removal efficiency of Au still had 90%.

doi:10.6342/NTU202002980

Therefore, TUACS is an excellent material for reuse in Au recovery from wastewater. This material could apply to the industry process and reduce the cost of recovery of the Au.

5.2 Suggestions

1. For material synthesized, several parameters remained unexamined in this study. The time and temperature for activation and the dosage of the thiourea used in modification have not yet optimized.

2. For adsorption experiments, the adsorption time to reach equilibrium needs 96 h, which was too long in industrial applications. The influence of adsorption temperature in adsorption kinetics should be further examined.

3. For desorption experiments, 24 h of desorption time was conducted, thus the optimal desorption time is not well known and should be further comprehended,

doi:10.6342/NTU202002980

Reference

Abbas, S. A., Forghani, M., Anh, S., Donne, S. W., & Jung, K. D. (2020). Carbon hollow spheres as electrochemical capacitors: Mechanistic insights. *Energy Storage Materials, 24*, 550-556.

Akcil, A., Erust, C., Gahan, C. S., Ozgun, M., Sahin, M., & Tuncuk, A. (2015). Precious metal recovery from waste printed circuit boards using cyanide and non-cyanide lixiviants – A review. *Waste Management, 45*, 258-271.

Alfarra, A., Frackowiak, E., & Béguin, F. (2004). The HSAB concept as a means to interpret the adsorption of metal ions onto activated carbons. *Applied Surface Science, 228*(1), 84-92.

Arima, H., Fujita, T., & Yen, W. T. (2002). Gold cementation from ammonium thiosulfate solution by zinc, copper and aluminium powders. *Materials transactions*, 43(3), 485-493.

Balakrishnan, T., & Ford, W. T. (1982). Particle size control in suspension copolymerization of styrene, chloromethylstyrene, and divinylbenzene. *Journal of applied polymer science*, 27(1), 133-138.

Baldé, C. P., Forti, V., Gray, V., Kuehr, R., & Stegmann, P. (2017). *The global e-waste monitor 2017: quantities, flows and resources*. Bonn/Geneva/Vienna: United Nations University (UNU), International Telecommunication Union (ITU) & International Solid Waste Association (ISWA).

Biniak, S., Szymański, G., Siedlewski, J., & Świątkowski, A. (1997). The characterization of activated carbons with oxygen and nitrogen surface groups. *Carbon, 35*(12), 1799-1810.

Birich, A., Raslan Mohamed, S., & Friedrich, B. (2018). Screening of Non-cyanide Leaching Reagents for Gold Recovery from Waste Electric and Electronic Equipment. *Journal of Sustainable Metallurgy, 4*(2), 265-275.

doi:10.6342/NTU202002980

Bryson, A. W. (1995). Gold Adsorption by Activated Carbon and Resin. *Mineral Processing and Extractive Metallurgy Review, 15*(1-4), 145-151.

Burg, P., Fydrych, P., Cagniant, D., Nanse, G., Bimer, J., & Jankowska, A. (2002). The characterization of nitrogen-enriched activated carbons by IR, XPS and LSER methods. *Carbon, 40*(9), 1521-1531.

Can, N., Ömür, B. C., & Altındal, A. (2016). Modeling of heavy metal ion adsorption isotherms onto metallophthalocyanine film. *Sensors and Actuators B: Chemical, 237*, 953-961.

Chen, Y., Zi, F., Hu, X., Yang, P., Ma, Y., Cheng, H.,Ma, Y., Wang, Q., Qin, X., Liu, Y., Chen, S., & Wang, C. (2020). The use of new modified activated carbon in thiosulfate solution: A green gold recovery technology. *Separation and Purification Technology, 230*, 115834.

Choudhary, B. C., Paul, D., Borse, A. U., & Garole, D. J. (2018). Surface functionalized biomass for adsorption and recovery of gold from electronic scrap and refinery wastewater. *Separation and Purification Technology, 195*, 260-270.

Chou, J., & McFarland, E. W. (2004). Direct propylene epoxidation on chemically reduced Au nanoparticles supported on titania. *Chemical communications*, (14), 1648-1649.

Cui, H., & Anderson, C. G. (2016). Literature review of hydrometallurgical recycling of printed circuit boards (PCBs). *Journal of Advanced Chemical Engineering*, *6*(1), 1-11.

Cyganowski, P., Garbera, K., Leśniewicz, A., Wolska, J., Pohl, P., & Jermakowicz-Bartkowiak, D. (2017). The recovery of gold from the aqua regia leachate of electronic parts using a core–shell type anion exchange resin. *Journal of Saudi Chemical Society, 21*(6), 741-750.

Da Silva, M. S., de Melo, R. A., Lopes-Moriyama, A. L., & Souza, C. P. (2019). Electrochemical extraction of tin and copper from acid leachate of printed circuit boards using copper electrodes. *Journal of Environmental Management*, 246, 410-417.

doi:10.6342/NTU202002980

Daud, W. M. A. W., & Ali, W. S. W. (2004). Comparison on pore development of activated carbon produced from palm shell and coconut shell. *Bioresource Technology, 93*(1), 63-69.

Derbyshire, F., Jagtoyen, M., Andrews, R., Rao, A., Martin-Gullon, I., & Grulke, E. A. (2001). Carbon materials in environmental applications. *Chemistry and physics of carbon*, 1-66.

Ding, Y., Zhang, S., Liu, B., Zheng, H., Chang, C. C., & Ekberg, C. (2019). Recovery of precious metals from electronic waste and spent catalysts: A review. *Resources, Conservation and Recycling, 141*, 284-298.

Dong, S., Alvarez, P., Paterson, N., Dugwell, D. R., & Kandiyoti, R. (2009). Study on the Effect of Heat Treatment and Gasification on the Carbon Structure of Coal Chars and Metallurgical Cokes using Fourier Transform Raman Spectroscopy. *Energy & Fuels, 23*(3), 1651-1661.

Dong, Z., Jiang, T., Xu, B., Yang, Y., & Li, Q. (2019). An eco-friendly and efficient process of low potential thiosulfate leaching-resin adsorption recovery for extracting gold from a roasted gold concentrate. *Journal of Cleaner Production, 229*, 387-398.

Dorfner, K. (Eds.). (1991). *Ion Exchangers*. Berlin, Boston: De Gruyter.

Fan, Y., Yang, X., Zhu, B., Liu, P. F., & Lu, H. T. (2014). Micro-mesoporous carbon spheres derived from carrageenan as electrode material for supercapacitors. *Journal of Power Sources, 268*, 584-590.

Fan, Z. J., Kai, W., Yan, J., Wei, T., Zhi, L. J., Feng, J., Ren, Y. M., Song, L. P., & Wei, F (2011). Facile synthesis of graphene nanosheets via Fe reduction of exfoliated graphite oxide. *ACS nano*,*5*(1), 191-198.

Gajdovcik, P., Lehocka, D., Duplákova, D., Botko, F., & Sitek, L. (2019). Design of Printed Circuit Board Production using Water Jet Technology. *TEM Journal, 8*(4), 1313-1318.

García-Soto, M. J., & González-Ortega, O. (2016). Synthesis of silica-core gold nanoshells and some modifications/variations. *Gold Bulletin*, 49(3-4), 111-131.

doi:10.6342/NTU202002980

Goldberg, S. (2015). Equations and Models Describing Adsorption Processes in Soils. *Chemical Processes in Soils, 8*, 489-517.

Gröger, H., Kind, C., Leidinger, P., Roming, M., & Feldmann, C. (2010). Nanoscale hollow spheres: microemulsion-based synthesis, structural characterization and container-type functionality. *Materials*, *3*(8), 4355-4386.

Ha, V. H., Lee, J. C., Huynh, T. H., Jeong, J., & Pandey, B. D. (2014). Optimizing the thiosulfate leaching of gold from printed circuit boards of discarded mobile phone. *Hydrometallurgy, 149*, 118-126.

Halli, P., Elomaa, H., Wilson, B. P., Yliniemi, K., & Lundström, M. (2017). Improved Metal Circular Economy-Selective Recovery of Minor Ag Concentrations from Zn Process Solutions. *ACS Sustainable Chemistry & Engineering, 5*(11), 10996-11004.

Harris, P. J., Liu, Z., & Suenaga, K. (2008). Imaging the atomic structure of activated carbon. *Journal of Physics: Condensed Matter, 20*(36), 362201.

Hekmat, F., Hosseini, H., Shahrokhian, S., & Unalan, H. E. (2020). Hybrid energy storage device from binder-free zinc-cobalt sulfide decorated biomass-derived carbon microspheres and pyrolyzed polyaniline nanotube-iron oxide. *Energy Storage Materials, 25*, 621-635.

Islam, A., Ahmed, T., Awual, M. R., Rahman, A., Sultana, M., Aziz, A. A., Monir, M. U., Teo, S. H., & Hasan, M. (2020). Advances in sustainable approaches to recover metals from e-waste-A review. *Journal of Cleaner Production, 244*, 118815.

Jermakowicz-Bartkowiak, D., & Kolarz, B. N. (2013). Anionits for precious metals recovery. *Polimery*, 7, 524.

Khanra, P., Kuila, T., Kim, N. H., Bae, S. H., Yu, D. S., & Lee, J. H. (2012). Simultaneous bio-functionalization and reduction of graphene oxide by baker's yeast. *Chemical Engineering Journal*, *183*, 526-533.

Kim, E. Y., Kim, M. S., Lee, J. C., & Pandey, B. D. (2011). Selective recovery of gold from waste mobile phone PCBs by hydrometallurgical process. *Journal of Hazardous Materials, 198*, 206-215.

doi:10.6342/NTU202002980

Kirubakaran, C. J., Krishnaiah, K., Seshadri, S. K. (1991). Experimental study of the production of activated carbon from coconut shells in a fluidized bed reactor. *Industrial & engineering chemistry research*, *30*(11), 2411-2416.

Korolev, I., Altınkaya, P., Halli, P., Hannula, P. M., Yliniemi, K., & Lundström, M. (2018). Electrochemical recovery of minor concentrations of gold from cyanide-free cupric chloride leaching solutions. *Journal of Cleaner Production, 186*, 840-850.

Krishna, R., Unsworth, T., & Edge, R. (2016). *Reference Module in Materials Science and Materials Engineering: Raman Spectroscopy and Microscopy*. Amsterdam, Holland: Elsevier.

Kubo, S., Demir-Cakan, R., Zhao, L., White, R. J., & Titirici, M. M. (2010). Porous Carbohydrate-Based Materials via Hard Templating. *ChemSusChem: Chemistry & Sustainability Energy & Materials*, *3*(2), 188-194.

Kumar, A., Holuszko, M., & Espinosa, D. C. R. (2017). E-waste: An overview on generation, collection, legislation and recycling practices. *Resources, Conservation and Recycling, 122*, 32-42.

Kunii, D., & Levenspiel, O. (2013). *Fluidization engineering.* Amsterdam, Holland: Elsevier.

Kwak, D. H., Han, S. B., Lee, Y. W., Park, H. S., Choi, I. A., Ma, K. B., Kim, M. C., Kim, S. J., Kin, D. H., Sohn, J. I., & Park, K. W. (2017). Fe/N/S-doped mesoporous carbon nanostructures as electrocatalysts for oxygen reduction reaction in acid medium. *Applied Catalysis B: Environmental*, 203, 889-898.

Lacoste-Bouchet, P., Deschênes, G., & Ghali, E. (1998). Thiourea leaching of a copper-gold ore using statistical design. *Hydrometallurgy, 47*(2), 189-203.

Laguna, A. (Ed.). (2008). Modern supramolecular gold chemistry: gold-metal interactions and applications. New York: John Wiley & Sons.

Johnson, R. D., & Arnold, F. H. (1995). The temkin isotherm describes heterogeneous protein adsorption. *Biochimica et Biophysica Acta (BBA) - Protein Structure and Molecular Enzymology*, 1247(2), 293-297.

doi:10.6342/NTU202002980

Li, H., Eksteen, J., & Oraby, E. (2018). Hydrometallurgical recovery of metals from waste printed circuit boards (WPCBs): Current status and perspectives – A review. *Resources, Conservation and Recycling, 139*, 122-139.

Li, J., & Zeng, X. (2012). 13 - Recycling printed circuit boards. In V. Goodship & A. Stevels (Eds.), *Waste Electrical and Electronic Equipment (WEEE) Handbook* (pp. 287-311). Cambridge, London: Woodhead Publishing.

Li, R., Deng, H., Zhang, X., Wang, J. J., Awasthi, M. K., Wang, Q., Xiao, R., Zhou, B., Du, J., & Zhang, Z. (2019). High-efficiency removal of Pb(II) and humate by a CeO_2–MoS_2 hybrid magnetic biochar. *Bioresource Technology, 273*, 335-340.

Li, S., Pasc, A., Fierro, V., & Celzard, A. (2016). Hollow carbon spheres, synthesis and applications – a review. *Journal of Materials Chemistry A, 4*(33), 12686-12713.

Li, X., Lau, S. P., Tang, L., Ji, R., & Yang, P. (2014). Sulphur doping: a facile approach to tune the electronic structure and optical properties of graphene quantum dots. *Nanoscale, 6*(10), 5323-5328.

Li, X., Zhang, C., Zhao, R., Lu, X., Xu, X., Jia, X., Wang, C., & Li, L. (2013). Efficient adsorption of gold ions from aqueous systems with thioamide-group chelating nanofiber membranes. *Chemical Engineering Journal, 229*, 420-428.

Li, Y., Lin, Y., Xu, Z., Wang, B., & Zhu, T. (2019). Oxidation mechanisms of H_2S by oxygen and oxygen-containing functional groups on activated carbon. *Fuel Processing Technology, 189*, 110-119.

Li, Y., & Shi, J. (2014). Hollow-structured mesoporous materials: chemical synthesis, functionalization and applications. *Advanced Materials, 26*(20), 3176-3205.

Lin, G., Wang, S., Zhang, L., Hu, T., Peng, J., Cheng, S., & Fu, L. (2018). Synthesis and evaluation of thiosemicarbazide functionalized corn bract for selective and efficient adsorption of Au(III) from aqueous solutions. *Journal of Molecular Liquids*, 258, 235-243.

doi:10.6342/NTU202002980

Lu, Y., & Xu, Z. (2016). Precious metals recovery from waste printed circuit boards: A review for current status and perspective. *Resources, Conservation and Recycling, 113*, 28-39.

Macías-García, A., Valenzuela-Calahorro, C., Gómez-Serrano, V., & Espínosa-Mansilla, A. (1993). Adsorption of Pb^{2+} by heat-treated and sulfurized activated carbon. *Carbon, 31*(8), 1249-1255.

McDougall, G. J., & Hancock, R. D. (1981). Gold complexes and activated carbon. *Gold Bulletin, 14*(4), 138-153.

Meghea, A., Rehner, H., Peleanu, I., & Mihalache, R. (1998). Test-fitting on adsorption isotherms of organic pollutants from waste waters on activated carbon. *Journal of radioanalytical and nuclear chemistry*, 229(1-2), 105-110.

Ng, C., Losso, J. N., Marshall, W. E., & Rao, R. M. (2002). Freundlich adsorption isotherms of agricultural by-product-based powdered activated carbons in a geosmin–water system. *Bioresource Technology*, *85*(2), 131-135.

Pallarés, J., González-Cencerrado, A., & Arauzo, I. (2018). Production and characterization of activated carbon from barley straw by physical activation with carbon dioxide and steam. *Biomass and Bioenergy*, 115, 64-73.

Pathania, D., Sharma, S., & Singh, P. (2017). Removal of methylene blue by adsorption onto activated carbon developed from Ficus carica bast. *Arabian Journal of Chemistry*, 10, S1445-S1451.

Rajagopal, R. R., Aravinda, L. S., Rajarao, R., Bhat, B. R., & Sahajwalla, V. (2016). Activated carbon derived from non-metallic printed circuit board waste for supercapacitor application. *Electrochimica Acta*, 211, 488-498.

Sahin, M., Akcil, A., Erust, C., Altynbek, S., Gahan, C. S., & Tuncuk, A. (2015). A Potential Alternative for Precious Metal Recovery from E-waste: Iodine Leaching. *Separation Science and Technology*, 50(16), 2587-2595.

doi:10.6342/NTU202002980

Song, Z., Duan, H., Li, L., Zhu, D., Cao, T., Lv, Y., Xiong, W., Wang, Z., Liu, M., & Gan, L. (2019). High-energy flexible solid-state supercapacitors based on O, N, S-tridoped carbon electrodes and a 3.5 V gel-type electrolyte. *Chemical Engineering Journal*, 372, 1216-1225.

Sposito, G. (1989). The Chemistry of Soils. Oxford, England: Oxford University Press.

Staunton, W. P. (2016). Carbon-in-pulp. In *Gold Ore Processing* (pp. 535-552). Amsterdam, Holland: Elsevier.

Štofková, M., & Štofko, M. (2002). Ion exchange resin use for Au and Ag separation from diluted solutions of thiourea. *Metalurgija*, 41(1), 33-36.

Sui, Z., Zhang, X., Lei, Y., & Luo, Y. (2011). Easy and green synthesis of reduced graphite oxide-based hydrogels. *Carbon*, 49(13), 4314-4321.

Tansel, B. (2017). From electronic consumer products to e-wastes: Global outlook, waste quantities, recycling challenges. *Environment International*, 98, 35-45.

Terzyk, A. P. (2001). The influence of activated carbon surface chemical composition on the adsorption of acetaminophen (paracetamol) in vitro: Part II. TG, FTIR, and XPS analysis of carbons and the temperature dependence of adsorption kinetics at the neutral pH. *Colloids and Surfaces A: Physicochemical and Engineering Aspects*, 177(1), 23-45.

Titirici, M. M., Thomas, A., & Antonietti, M. (2007). Replication and coating of silica templates by hydrothermal carbonization. *Advanced functional materials*, 17(6), 1010-1018.

Tsai, C. Y., & Chiu, C. C. (2007). A case-based reasoning system for PCB principal process parameter identification. *Expert Systems with Applications*, 32(4), 1183-1193.

Wang, X. S., & Qin, Y. (2005). Equilibrium sorption isotherms for of Cu2+ on rice bran. *Process Biochemistry*, 40(2), 677-680.

Wang, Z. D., Yoshida, M., & George, B. (2013). Theoretical study on the thermal decomposition of thiourea. *Computational and Theoretical Chemistry*, 1017, 91-98.

doi:10.6342/NTU202002980

Wang, Z., Zhang, B., Ye, C., & Chen, L. (2018). Recovery of Au(III) from leach solutions using thiourea functionalized zeolitic imidazolate frameworks (TU*ZIF-8). *Hydrometallurgy*, 180, 262-270.

Wu, S. H., & Pendleton, P. (2001). Adsorption of Anionic Surfactant by Activated Carbon: Effect of Surface Chemistry, Ionic Strength, and Hydrophobicity. *Journal of Colloid and Interface Science*, 243(2), 306-315.

Wu, Z., Yuan, W., Li, J., Wang, X., Liu, L., & Wang, J. (2017). A critical review on the recycling of copper and precious metals from waste printed circuit boards using hydrometallurgy. *Frontiers of Environmental Science & Engineering*, 11(5), 8.

Xie, F., Lu, D., Yang, H., & Dreisinger, D. (2014). Solvent Extraction of Silver and Gold From Alkaline Cyanide Solution with lix 7950. *Mineral Processing and Extractive Metallurgy Review*, 35(4), 229-238.

Yang, C., Li, J., Tan, Q., Liu, L., & Dong, Q. (2017). Green Process of Metal Recycling: Coprocessing Waste Printed Circuit Boards and Spent Tin Stripping Solution. *ACS Sustainable Chemistry & Engineering*, 5(4), 3524-3534.

Yang, Y., Xue, M., Xu, Z., & Huang, C. (2013). Health risk assessment of heavy metals (Cr, Ni, Cu, Zn, Cd, Pb) in circumjacent soil of a factory for recycling waste electrical and electronic equipment. *Journal of Material Cycles and Waste Management*, 15(4), 556-563.

Young, C., Gow, N., Melashvili, M., & LeVier, M. (2012). Impregnated activated carbon for gold extraction from thiosulfate solutions. *Separation Technologies for Minerals, Coal, and Earth Resources*, 391.

Yu, H., Zi, F., Hu, X., Nie, Y., Chen, Y., & Cheng, H. (2018). Adsorption of gold from thiosulfate solutions with chemically modified activated carbon. *Adsorption Science & Technology,* 36(1-2), 408-428.

Yu, H., Zi, F., Hu, X., Nie, Y., Xiang, P., Xu, J., & Chi, H. (2015). Adsorption of the gold–thiosulfate complex ion onto cupric ferrocyanide (CuFC)-impregnated activated carbon in aqueous solutions. *Hydrometallurgy*, 154, 111-117.

doi:10.6342/NTU202002980

Zhan, L., & Xu, Z. (2014). State-of-the-Art of Recycling E-Wastes by Vacuum Metallurgy Separation. *Environmental Science & Technology*, 48(24), 14092-14102.

Zhang, Y. N., Ye, Z. F., Yang, K., & Dong, S. L. (2014). Antenna-predominant and male-biased CSP19 of Sesamia inferens is able to bind the female sex pheromones and host plant volatiles. *Gene*, 536(2), 279-286.

Zhang, Y., Liu, S., Xie, H., Zeng, X., & Li, J. (2012). Current Status on Leaching Precious Metals from Waste Printed Circuit Boards. *Procedia Environmental Sciences*, 16, 560-568.

Zhu, C., Guo, S., Fang, Y., & Dong, S. (2010). Reducing sugar: new functional molecules for the green synthesis of graphene nanosheets. *ACS nano*, 4(4), 2429-2437.

doi:10.6342/NTU202002980